Differences Between Severe and Nonsevere Warm -Season, Nocturnal Bow Echo Environments

Ezio L. Mauri and William A. Gallus, Jr.

Department of Geological and Atmospheric Sciences

Iowa State University

Ames, IA 50011

Submitted to *Weather and Forecasting* on 5 August 2020

Revision submitted 14 November 2020

Corresponding author address : Ezio Luca Mauri, Iowa State University, 3018 Agronomy Hall, Ames, IA 50011

E-mail: emauri@iastate.edu

Early Online Release: This preliminary version has been accepted for publication in *Weather and Forecasting*, may be fully cited, and has been assigned DOI 10.1175/WAF-D-20-0137.1. The final typeset copyedited article will replace the EOR at the above DOI when it is published.

ABSTRACT

Nocturnal bow echoes can produce wind damage, even in situations where elevated convection occurs. Accurate forecasts of wind potential tend to be more challenging for operational forecasters than for daytime bows because of incomplete understanding of how elevated convection interacts with the stable boundary layer. The present study compares the differences in warm-season, nocturnal bow echo environments in which high intensity (>70 knots) severe winds (HS), low intensity (50-55 knots) severe winds (LS), and nonsevere winds (NS) occurred. Using a sample of 132 events from 2010 to 2018, 43 forecast parameters from the SPC mesoanalysis system were examined over a 120 x 120 km region centered on the strongest storm report or most pronounced bowing convective segment. Severe composite parameters are found to be among the best discriminators between all severity types, especially Derecho Composite Parameter (DCP) and Significant Tornado Parameter (STP). Shear parameters are significant discriminators only between severe and nonsevere cases, while Convective Available Potential Energy (CAPE) parameters are significant discriminators only between HS and LS/NS bow echoes. Convective Inhibition (CIN) is among the worst discriminators for all severity types. The parameters providing the most predictive skill for HS bow echoes are STP and most unstable CAPE, and for LS bow echoes are V wind component at best CAPE (VMXP) level, STP, and Supercell Composite Parameter. Combinations of two parameters are shown to improve forecasting skill further, with the combination of surface-based CAPE and 0 – 6 km U shear component, and DCP and VMXP, providing the most skillful HS and LS forecasts, respectively.

Accepted for publication in *Weather and Forecasting*. DOI 10.1175/WAF-D-20-0137.1.

1. Introduction

Bow echoes (Fujita 1978; Johns 1993; Weisman 1993; Przybylinski 1995), a subset of mesoscale convective systems (MCSs), frequently generate damaging straight-line surface winds (Fujita and Wakimoto 1981; Davis et al. 2004; Ashley and Mote 2005; Atkins et al. 2005; Wheatley et al. 2006; Wakimoto et al. 2006). These events account for the majority of casualties and damage resulting from convective nontornadic winds in the United States (Johns and Hirt 1987; Przybylinski 1995; Davis et al. 2004; Ashley and Mote 2005). Therefore, forecasting these types of storms correctly is essential to reduce risk to lives and property.

Idealized simulations by Weisman (1993) suggested that severe, long-lived bow echoes (i.e., derechos; see Corfidi et al. (2016) for the precise definition of a derecho) may be generated in environments with Convective Available Potential Energy (CAPE) of at least 2000 m^2 s^{-2} and vertical wind shear of at least 20 m s^{-1} over the lowest 5 km above ground level (AGL). Coniglio et al. (2004) stressed the importance of low-level moisture (James et al. 2006; Guastini and Bosart 2016) and relatively dry conditions at midlevels, and the detrimental effect of low instability and weak deep-layer shear on bow echoes. Contrary to Weisman (1993), Evans and Doswell (2001), and Coniglio et al. (2004) found low-level (0-2.5 km) shear not skillful in forecasting long-lived bow echoes. Evans and Doswell (2001) found high variation in the ambient shear and instability (similar to Coniglio et al. 2004; Cohen et al. 2007), suggesting that, alone, they are not sufficient to differentiate derecho environments from those associated with nonsevere MCSs.

Cohen et al. (2007) investigated nonsevere MCSs, severe MCSs, and severe derecho-producing MCSs and found that the best discriminators for distinguishing severe wind-producing

Accepted for publication in *Weather and Forecasting*. DOI 10.1175/WAF-D-20-0137.1.

MCSs from nonsevere MCSs were deep-layer wind shear and low- to upper-level wind speeds, together with median 0-1 km system-relative wind speeds and midlevel environmental lapse rates. Similar to Johns and Doswell (1992), they found that low-level (0-2 km) wind shear is a worse discriminator compared to deep-layer (0–6 km and 0–10 km) shear. Moreover, they observed that vertical differences in equivalent potential temperature and CAPE only differentiate well between weak and severe/derecho MCS environments; environments characterized by downdraft CAPE (DNCP; the maximum energy available to a descending parcel) over 1000 J kg-1 are favorable for severe wind-producing mesoscale convective systems, which agrees with Evans and Doswell (2001).

Despite the fact MCSs are common at night, it might be assumed that bow echoes with damaging winds are rare at night, since these environments are often characterized by a nocturnal stable boundary layer (SBL; Schultz et al. 2000). SBLs should hinder - or even impede in certain cases – the generation of strong cold pools with tight temperature and pressure gradients more so than what occurs during the daytime, and could potentially reduce momentum transport to the ground within negatively buoyant downdrafts (Horgan et al. 2007). However, bow echoes and intense derechos often occur at night (Johns and Hirt 1987; Bentley and Mote 1998; Bernardet and Cotton 1998; Davis et al. 2004; Wakimoto et al. 2006; Wheatley et al. 2006; Adams-Selin and Johnson 2010; Coniglio et al. 2012; Adams-Selin and Johnson 2013; Guastini and Bosart 2016). These nocturnal bow echoes, and more generally MCSs, are more poorly forecast compared to daytime convective systems (Davis et al. 2003, Wilson and Roberts 2006; Clark et al. 2007; Weisman et al. 2008; Hitchcock et al. 2019; Weckwerth et al. 2019), possibly because nocturnal convection is often elevated, with forcing mechanisms above the ground, such as convergence at the nose of the low-level jet (LLJ; e.g., Stull 1988), gravity waves, or bores,

Accepted for publication in *Weather and Forecasting*. DOI 10.1175/WAF-D-20-0137.1.

being more important than during the daytime. Therefore, the relative lack of observations above the surface is more of a problem at night because it would be these observations that would show the areas likely to produce sufficient lift to trigger elevated thunderstorms (Davis et al. 2003; Clark et al. 2007; Hitchcock et al. 2019).

Nocturnal bow echo environments are often characterized by an SBL and a LLJ, which provide an elevated source of moist and unstable air and creates a favorable environment for MCSs (e.g., Corfidi et al. 2008; Schumacher and Johnson 2009; French and Parker 2010; Blake et al. 2017). These nocturnal systems are often elevated (Colman 1990, Parker 2008), in environments with considerable surface-based CIN (Convective Inhibition; SBCN), due to the disconnect of the SBL and unstable air aloft, thus only ingesting air parcels located above the SBL. While the regeneration of convective cells at the leading edge of a cold pool typically maintains daytime MCSs (Rotunno et al. 1988), some studies have found that nocturnal MCSs can also be cold-pool driven and surface-based despite it being more difficult for a strong cold pool to develop at night (Parker 2008; Marsham et al. 2011; Peters and Schumacher 2016; Parker et al. 2020), due to the strength of the SBL, increased temperature homogeneity, and/or reduced evaporative cooling in the tropospheric layer just above the ground. However, other studies indicate that bores (e.g., Crook 1988; Wilson and Roberts 2006; Haghi et al. 2017) or gravity waves (e.g., Crook and Moncrieff 1988; Parker 2008; Marsham et al. 2010) generated by weak cold pools play a key role to sustain nocturnal MCSs (Crook and Moncrieff 1988; Koch et al. 2008; Parker 2008; French and Parker 2010; Marsham et al. 2010; Marsham et al. 2011; Blake et al. 2017; Parsons et al. 2019).

At the present time, shortcomings exist in our understanding of which processes allow severe convective winds to reach the surface in stable environments. Parker (2008) investigated

Accepted for publication in *Weather and Forecasting*. DOI 10.1175/WAF-D-20-0137.1.

severe convective winds in stable environments and found that even in the absence of surface-based CAPE, elevated convective systems could generate negatively-buoyant downdrafts strong enough to reach the surface. Marsham et al. (2011) investigated an MCS, whose initial convection triggered both gravity waves and bores, which initiated further convection ahead of the cold pool that became surface based. Hitchcock et al. (2019) found that out of 13 MCSs sampled by PECAN (Plains Elevated Convection at Night; Geerts et al. 2017), almost every postconvective nocturnal sounding observed a surface cold pool, suggesting that the potential for damaging surface winds associated with nocturnal MCSs may be higher than expected. Recently, Parker et al. (2020) conducted an idealized simulation of the nocturnal PECAN MCS that occurred on 26 June 2015 and observed that initially elevated convection became surface based, and severe surface winds were produced. However, this binary distinction between surface-based and elevated convection is relatively ambiguous, as nocturnal MCSs exist on a spectrum between these two extremes, i.e., they may ingest SBL air from different source layers (Corfidi et al. 2008).

Considering the gaps in our understanding of how elevated convection interacts with the SBL, nocturnal severe wind-producing storms can present a challenge for operational forecasters. Being able to discriminate between environments in which a nocturnal bow echo cannot generate intense surface winds from environments where it will produce severe winds is an important societal and scientific question to answer. Although nocturnal bow echoes can produce severe winds at the surface, there is a dearth of studies in the literature that specifically analyze nocturnal bow echoes (Wakimoto et al. 2006). Therefore, the goal of this project is to examine the differences in near-storm parameters between warm-season, nocturnal bow echoes that produce severe winds and those that do not.

Accepted for publication in *Weather and Forecasting*. DOI 10.1175/WAF-D-20-0137.1.

A description of the data and methods is presented in the following section. Section 3 discusses single and multiple parameters results. General summary and conclusions are presented in section 4.

2. Data and methodology

a. Data collection and classification

The analysis of the environmental conditions associated with bow echoes varying in severity was conducted by selecting a sample of 132 warm-season, nocturnal bow echo events occurring during the April-August period each year from 2010 to 2018 (see the online supplemental material). In the present study, cases were considered nocturnal if a bowing convective line was present between 02 UTC and 11 UTC. These events were chosen using composite reflectivity data from the UCAR Image Archive browser (https://www2.mmm.ucar.edu/imagearchive). A loop of composite reflectivity for the contiguous United States was examined and, when bow echoes were noted, if the criteria explained below were met, the cases were used in the study. Although a few bow echoes meeting the criteria may have been missed, the majority of all relevant events were captured.

Included in this sample were 44 nonsevere cases (NS) in which there were no measured severe winds or wind damage reports for at least six hours before and after the time of maximum bow echo development (largest area within bow of reflectivity greater than 50 dBZ). Of the remaining 88 cases, 41 were low-intensity severe wind cases (LS), where all wind reports were in the range of 50-55 kt, and 47 were high-intensity severe winds cases (HS), where at least one

Accepted for publication in *Weather and Forecasting*. DOI 10.1175/WAF-D-20-0137.1.

severe wind report with a magnitude greater than 70 kt occurred. Therefore, this classification is more focused on wind intensity than Cohen et al. (2007), who classified MCSs based on the number of reports of severe winds rather than severity, and assumed that weak nonsevere MCSs could have up to 5 storm reports. The present study, like Cohen et al. (2007), used both estimated and measured wind reports. It is well known that deficiencies exist in the wind database, such as the human tendency to overestimate wind speeds (Edwards et al., 2018). However, it was necessary to include both types of reports to maintain a sufficient sample size for meaningful analysis.

The analysis focuses on SPC mesoanalysis-derived proximity soundings to represent the storm environment (Evans and Doswell 2001; Doswell and Evans 2003; Coniglio et al. 2004; Cohen et al. 2007; Thompson et al. 2012; Reames 2017). The General Meteorology Package (GEMPAK) software (desJardins et al. 1991) was used to obtain a set of 43 sounding-derived parameters from the 40-km horizontal grid spacing SPC mesoanalysis system (Table 1; Bothwell et al. 2002; Coniglio et al. 2012). This dataset is based upon the hourly 40-km RUC, and after May 2012, 40-km RAP, analysis grids, adjusted using surface observations, which is known at the Storm Prediction Center as *SFCOA* (surface objective analysis) and on the SPC website as *mesoanalysis*. The selected parameters include measures of vertical wind shear, wind speed, multiple thermodynamic properties and also four composite indices. These four indices are the Supercell Composite Parameter (SCP; Thompson et al. 2004), a function of effective storm relative helicity (SRH; based on Bunkers right supercell motion, Bunkers et al. 2000), most unstable CAPE (MUCP), most unstable CIN (MUCN), and 0-6 km shear magnitude (S6MG); Significant Tornado Parameter (STP; Thompson et al. 2012), using surface-based CAPE (SBCP), 0-1 km SRH (SRH1), and S6MG; Derecho Composite Parameter (DCP; Evans and

Accepted for publication in *Weather and Forecasting*. DOI 10.1175/WAF-D-20-0137.1.

Doswell 2001), a function of downdraft CAPE (DNCP), MUCP, S6MG, and the 0-6 km mean wind; and XTRN, the product of maximum mixing ratio (MXMX) and wind speed at the most unstable parcel level (MUPL).

For severe cases, the mesoanalysis data at the nine grid points, a 3x3 grid, closest to the wind report of the largest magnitude within the ranges specified earlier and using the analysis hour immediately before the report occurred were averaged. To properly examine the environment associated with bow echoes and prevent previous convection from skewing results, if the storm report was within ten minutes after the analysis time, the previous hour (60-70 minutes earlier) was used instead. For NS cases, the mesoanalysis data were averaged from the nine grid points, a 3x3 grid, closest to the apex of the bow (i.e., where the strongest winds typically occur; Weisman 2003; Atkins and St. Laurent 2009), and at the analysis hour immediately prior to the maximum bow echo development on radar, to avoid having prior convection alter the environmental parameters. Additionally, earlier radar images were examined for a 10-hour period over a roughly 200x200 km region ahead of the bow echo to ensure that the environment was not influenced by prior unrelated convection. All storms occurred east of the Rocky Mountains, and the three severity types were well spatially distributed across primarily the central United States (Fig. 1), reducing the potential for regional biases. The seasonal distribution of cases was also similar among the three severity types (not shown).

b. Statistical methods

To analyze forecast parameters, several graphical and statistical techniques were employed. Means, medians, bias, interquartile distribution, box-and-whiskers plots, and scatter

Accepted for publication in *Weather and Forecasting*. DOI 10.1175/WAF-D-20-0137.1.

plots were used to obtain additional information and to easily visualize features in the data such as clusters, trends, spread, and outliers. The significance of the differences among the parameter distributions and the discriminatory ability of a specific variable were determined using bootstrapped paired t-tests (Mendenhall and Sincich 2007) and non-parametric Wilcoxon signed rank-sum tests (Wilks 2011). A significance level of $p = 5\%$ was used to determine if a test statistic was statistically significant. Since the results of the two tests were very similar, with only about 5% of parameters found to be significant with one test but not the other, only the bootstrapped paired t-tests are presented in the results to follow.

Additionally, the Heidke Skill Score (hereafter HSS; Heidke 1926) and threshold values were calculated to provide a more robust quantitative analysis about the forecasting skill of the parameters. The HSS is defined as

$$HSS = 2\frac{ad - bc}{(a + c)(c + d) + (a + b)(b + d)}$$

where a, b, c, and d are the hits, false alarms, misses, and correct rejections, respectively. An HSS of 1 indicates all forecasts are correct, 0 indicates that the forecast has no skill, and negative values indicate that a chance forecast is better.

Similar to Kuchera and Parker (2006) for severe convective winds and Reames (2017) for tornadoes, optimal threshold values, $x_{opt,i}$, are obtained by maximizing the HSS. An HS event would be forecast if the value of a forecast parameter is greater than $x_{opt,1}$, whereas for an NS event it would be lower than $x_{opt,2}$; for the average relative humidity from LCL to 500 hPa (RHC5) and from LCL to LFC (RHLC), the average kinematic vertical velocity between MUPL and LCL (VKLC), the 3 km average relative humidity (3KRH), the relative humidity at 800 hPa (RH80) and 700 hPa (RH70), the reverse is true for both severity types. An LS event would be forecast if the value of a forecast parameter is between the range $x_{opt,3}$ and $x_{opt,4}$. The same

Accepted for publication in *Weather and Forecasting*. DOI 10.1175/WAF-D-20-0137.1.

method was used in the case of any combination of two parameters, with the addition that the same condition needed to apply to both parameters: for instance, an HS event would be forecast if both forecast parameters exceed the two new optimal thresholds $x_{opt,5}$ and $x_{opt,6}$ in the appropriate direction (Reames 2017).

To analyze the two-dimensional severe weather parameter spaces, the Gaussian kernel density estimation (GKDE; Scott 2015) was used, which was performed for two-dimensional probability analyses considering combinations of multiple parameters. The GDKE is a method to estimate the multivariate probability density function of two random variables in a non-parametric way, which allows one to gain knowledge about the continuous distribution of data where no observed data points exist. This method has also been implemented to create continuous probabilistic fields of significant severe storm report locations (Smith et al. 2012), tornadic near-storm environmental characteristics for convective mode (Thompson et al. 2012), and tornadic environments in the two-dimensional convective parameter spaces (Reames 2017). Many of the parameters examined in the present study have been shown to be useful in distinguishing convective mode and observed severe weather (Johns et al. 1993; Brooks et al. 1994; Evans and Doswell 2001; Doswell and Evans 2003; Thompson et al. 2003; Kuchera and Parker 2006; Thompson et al. 2012; Hampshire et al. 2017; Reames 2017).

3. Results

The following analyses compare the distributions of near-storm environmental parameters and thermodynamic soundings between HS, LS, and NS nocturnal events. In the results presented below, all differences to be discussed were found to be statistically significant

Accepted for publication in *Weather and Forecasting*. DOI 10.1175/WAF-D-20-0137.1.

unless otherwise noted. In addition, the skill of both single parameters and combinations of parameters as forecasting tools in discriminating different severity types is evaluated.

a. Single parameter distributions

Many prior studies (e.g., Rotunno et al. 1988; Weisman and Rotunno 2004; Coniglio et al. 2006; Cohen et al. 2007; Coniglio et al. 2012) have commented on the importance of vertical wind shear on the initiation and maintenance of deep moist convection and bow echoes. We find that shear, whether it is present in low levels or deeper levels, discriminates well between nonsevere events and severe events (Fig. 2; Table 2). The differences in the mean values between the shear variables can also be seen in Table 1. NS environments are associated with significantly weaker low-level, mid-level, and upper-level wind shear than severe ones for all the shear parameters examined. This is also true for low-level SRH by as much as 100 $m^2 s^{-2}$. When discriminating between LS and HS environments, shear measures in the lowest layers (0-1 km and 0-3 km) show rather minor insignificant differences (similar to Evans and Doswell 2001; Cohen et al. 2007). As one considers deeper layers of shear (0-6 km and 0-8 km) there is more separation between the medians shown in the boxplots (similar to Coniglio et al. 2006; Cohen et al. 2007), but it is not statistically significant. An exception does exist for the 0-6 km (U6SV) and 0-8 km pressure-weighted (U8SV) U shear components. Differences in these two parameters were not significant at the 95% confidence level, but were significant at the 90% level (not shown). The value of S6MG for HS events (41.1 kt; Table 1) is similar to that found for derecho-producing MCSs by Cohen et al. (2007; about 43 kt) and Coniglio et al. (2004; around 40 kt), while that for LS events is 36.9 kt. The U shear component in the 0-3 km layer does not differ

Accepted for publication in *Weather and Forecasting*. DOI 10.1175/WAF-D-20-0137.1.

much between severity types, but differs more noticeably for deeper 0-6 km and 0-8 km shear, with the most intense nocturnal bow echo winds happening with the strongest zonal shear component. As is shown later, this increasing zonal component to the shear is primarily due to stronger zonal winds aloft. Additionally, the meridional component of the wind differs significantly in the lowest layer between the nonsevere and severe events; however, the differences among all three severity types were not significant in the deeper layers (and thus are not plotted). VKLC is also a significant discriminator between severe and nonsevere cases (figure not shown), and between HS and LS events at the 90% confidence level. Greater lift in the near-storm environment has multiple effects: it can help cool the mid-troposphere increasing the CAPE available for storms, and it may allow for longer sustenance of convection or provide more favorable conditions for upscale growth. These factors may facilitate the occurrence of severe winds.

Nocturnal HS bow echo environments are characterized by the highest values of SBCP (1518 J kg^{-1}), 100 hPa mean mixed CAPE (M1CP; 1605 J kg^{-1}), MUCP (2363 J kg^{-1}), and DNCP (1025 J kg^{-1}) compared to both the LS and NS ones, greater by nearly 1000 J kg^{-1} for SBCP and MUCP (Table 1), making them very good parameters for discriminating between HS and LS/NS (Fig. 3; Table 2). In addition, we find that CAPE is not a good discriminator between NS and LS environments. These findings somewhat contrast with those found by Cohen et al. (2007), who found that CAPE can only discriminate well between weak and severe/derecho MCS environments, but not severe vs derecho-producing MCSs. DNCP increases with increasing bow echo intensity, as found by Evans and Doswell (2001) and Cohen et al. (2007); values greater than 1000 J kg^{-1} have been associated with increasing potential for strong downdrafts and damaging outflow winds (James et al. 2006). Increased values of CAPE and DNCP are found to

Accepted for publication in *Weather and Forecasting*. DOI 10.1175/WAF-D-20-0137.1.

be a distinctive trait of HS bow echoes, suggesting that the nocturnal SBL may not be as cool in these events, making it easier for a cold pool to reach the ground and produce damaging winds (Parker et al. 2020). However, for our sample of cases, CIN is among the worst discriminators overall, as values among all severe environments are relatively similar (Fig. 3). Mean values show that SBCN and MUCN are in fact highest for LS events (Table 1). The finding that CIN does not distinguish well between the severity types may be consistent with the results of Parker et al. (2020) and Hiris and Gallus (2020), who found that the presence of low-level stable layers in idealized experiments using CM1 (Bryan and Fritsch 2002) does not prevent the formation of cold pools nor upscale growth of convection. Furthermore, almost all observed MCSs during the recent PECAN project contained at least a weak surface cold pool, even when a stable boundary layer was also observed (Hitchcock et al. 2019).

Comparatively dry conditions characterize HS environments at 700 hPa (Fig. 4), agreeing with prior works suggesting dry air around this level encourages evaporative cooling and strong negative buoyancy, and thus is a favorable ingredient for strong downdrafts (e.g., Johns 1993). While RH70 discriminates only between HS and LS/NS types, RH80 discriminates between HS and LS, and RHC5 between HS and NS. Relative humidity at the levels examined is not able to differentiate between LS and NS events. The results for relative humidity suggest that the HS events are the ones that may be most influenced by enhanced evaporative cooling and stronger downdrafts that greatly accelerate the flow, whereas other processes may play a bigger role in determining whether or not a storm produces weaker severe winds. The highest LCLs are associated with HS environments (608 m), but differences compared to the other severity types are not significant. Since LCL height is a function of the relative humidity in the layer closest to the ground, and these events are nocturnal with SBLs present so that the relative humidity near

Accepted for publication in *Weather and Forecasting*. DOI 10.1175/WAF-D-20-0137.1.

the ground would likely be relatively high in all events, it is not surprising that LCL heights would not differ significantly among the three severity types. While the maximum equivalent potential temperature (theta-e) difference in lowest 3 km (TE3K) differentiates well between severe and nonsevere environments, surface theta-e (STHE) differentiates best between HS and LS/NS environments (Table 2).

As in Craven and Brooks (2004), lapse rates exceeding 7° C km^{-1} are classified as steep in the present study. The lapse rate from 850 to 500 hPa (LR85) and from 700 to 500 hPa (LR75) discriminate significantly between severe and nonsevere cases (Table 2). In addition, LR75 performs well also when comparing HS (steep lapse rate, 7.27° C km^{-1}) and LS (6.89° C km^{-1}) (Fig. 4), suggesting that steeper lapse rates in this layer contribute to the higher values of CAPE parameters for HS events. Maximum mixing ratio (MXMX in Table 1) is highest for HS events, also consistent with higher CAPE when considering the steeper lapse rates, and it discriminates between HS vs NS/LS. The composite parameter XTRN differentiates well between severe and nonsevere cases (figure not shown). We believe that this is mainly because stronger wind shear leads to higher XTRN values, and as will be shown later, stronger winds are associated with more intense convection.

The highest values of the severe composite parameters SCP, STP, and DCP occur in HS environments (8.55, 1.11, 3.48 respectively), followed by LS, and then NS ones (Table 1). Separation between all severity types is substantial (Fig. 5) and all parameters differentiate significantly among all three severity types (Table 2). It is likely that SCP, STP, and DCP work so well because they all include at least one parameter that discriminates significantly between severe and nonsevere (e.g., shear, SRH), and at least one that discriminates well between HS and LS/NS (e.g., CAPE). The DCP identifies favorable environments for cold-pool driven wind

Accepted for publication in *Weather and Forecasting*. DOI 10.1175/WAF-D-20-0137.1.

events (Evans and Doswell 2001, Lagerquist et al. 2017), and values greater than 2 favor the development of derechos from existing MCSs (Lagerquist et al. 2017). We find that DNCP, related to the potential for cold-pool production, LR75, SCP, STP, and DCP are the parameters among the 43 examined that discriminate significantly among all three severity types. For brevity, only parameters for which any comparison showed statistically significant differences (31 of the 43 studied) are included in the analyses to follow. Removing parameters with $p \geq 5\%$ does not imply that a parameter is unimportant for distinguishing between bow echo severity types, only that it cannot statistically differentiate between the types. For LS vs NS nocturnal environments (Table 2), 21 parameters (48%) were retained after testing; for HS vs NS, 28 parameters (65%), and for HS vs LS, 12 parameters (27%) were retained.

Soundings averaged for all events in each severity class (Fig. 6) were computed using the original 40-km RUC/RAP analyses, and thus some parameters may differ slightly from the SPC mesoanalysis. In Fig. 6, the parcel trajectory for the most-unstable parcel is shown since MUCP was found to differentiate the best among CAPE parameters between HS and LS/NS in the SPC mesoanalyses. The soundings indicate that lower values of RH70 for HS and LS are due to both a warmer and drier environment at that level. The soundings also show that the lower troposphere is warmer and moister in HS events than in other events, likely the primary reason for the higher CAPE values in those cases discussed earlier. Winds at 500 hPa are about 20 kt for NS, 30 kt for LS, and 35 kt for HS environments, which is less than the 41 kt found by Johns and Hirt (1987), and have a stronger southerly component for severe events. The average soundings are shown using 950 hPa as an assumed surface point, since the average surface pressure of all cases is 951 hPa (948.6 hPa for NS, 953.5 hPa for LS, and 953.6 for HS), and data are only available every 25 hPa. The portion of the soundings nearest the ground should be interpreted

Accepted for publication in *Weather and Forecasting*. DOI 10.1175/WAF-D-20-0137.1.

with caution since the soundings used to create these average soundings have different surface elevations. Therefore, to better examine differences in the SBL near the ground for different severity types, a separate analysis of the depth of the SBL was performed (Fig. 7). The depth was determined to be the top of the layer where the lapse rates were more stable than a moist adiabatic lapse rate. This analysis supports the results found for CIN variables, in that the depths of the SBLs do not differ among the three severity types. The majority (over 60%) of SBLs are shallower than 50 hPa, less than 10% are deeper than 100 hPa, and only about 10% are unstable for all severity types.

In summary, while many parameters involving shear, helicity, wind speeds, and thermodynamics were found to differ significantly between NS events and severe ones, only a few thermodynamic parameters and three composite indices differed significantly between the HS and LS events. These results suggest that, while many kinematic, shear-based, and thermodynamic quantities can help forecasters differentiate between severe and nonsevere nocturnal bow echo environments, only severe composite indices and some thermodynamic variables can help differentiate environments likely to produce bow echoes with high intensity severe wind from ones that will only produce marginally-severe wind.

b. Nocturnal distribution analysis

The nocturnal frequency distribution by hour for each severity type used in the present study (Fig. 8) peaks at 02 UTC for HS and LS types and at 03 UTC for NS types, and shows that our dataset is relatively evenly distributed, with many events also occurring later in the night. The single report at 01 UTC is due to a case where the report was within the ten

Accepted for publication in *Weather and Forecasting*. DOI 10.1175/WAF-D-20-0137.1.

minutes after the 02 UTC analysis time, and, as explained earlier, this meant that the 01 UTC mesoanalysis information was used. To ensure that typical nocturnal trends in parameters are not the primary cause of differences between the severity levels (such as would happen, for instance, if HS cases occurred more frequently early in the evening when CAPE is higher, whereas NS events dominated later at night when CAPE is lower), the sample was divided into two groups of similar size: one before 05 UTC (late evening) and one after 05 UTC (early morning). The analysis was repeated separately for the two subsets of cases, comprising 65 total events for late evening, of which 23 were HS, 24 LS, and 18 NS, and 67 total events for early morning, of which 24 were HS, 17 LS, and 26 NS. The two subsets are generally similarly distributed among the three severity types. For late evening comparisons between LS and NS bow echo environments 17 parameters were retained after bootstrap testing (39% of initial parameters), while 14 (32%) were retained for early morning and 21 for the whole sample. For differences between HS and NS 21 parameters were kept (49%) for late evening, while 25 (58%) were for early morning and 28 for the whole night. For differences between HS and LS, 13 parameters were retained (30%), while 6 (14%) were for early morning and 12 for the whole dataset. In the following analysis, the surface V wind component (VWND), U component at the top of the effective inflow layer (UEIL), and RH80 are not shown since no statistically significant differences were found for any of the three comparisons between severity types for either time period.

When separated into the two different time periods (Table 3), the majority of SRH and shear parameters behave as they did for the full sample and remain good discriminators between severe and nonsevere types, regardless of the time period chosen (Table 4), with substantial separation in the distributions of values (Fig. 9). None of the kinematic parameters differentiate

Accepted for publication in *Weather and Forecasting*. DOI 10.1175/WAF-D-20-0137.1.

between HS and LS types (except for VKLC during late evening). The fact that kinematic parameters do not differentiate between the intensity of the winds in severe cases, but relative humidity did, again implies the important role that evaporative cooling might play in the creation of downdrafts that are able to substantially accelerate the flow in HS events. The 0-3 km U (U3SV) and V (V3SV) shear components are good discriminators between severe and nonsevere types only during early morning. S6MG, U6SV, and U8SV discriminate between LS and NS events only during late evening, but distinguish between HS and NS for both time periods. All HS SRH and shear mean values are larger during early morning than late evening, possibly reflecting the fact that the nocturnal LLJ typically peaks in intensity during this period, and that the surface layer would be most likely to be decoupled from the flow aloft in the early morning.

As would be expected, since CAPE is a function of low-level temperature and the lower troposphere still possesses some of the warming from the solar radiation prior to sunset, mean values for all CAPE parameters are higher during late evening than in early morning (Table 3), with the differences being statistically significant for SBCP and DNCP for HS cases. Differences between the periods before and after 05 UTC grow larger as severity increases, with the biggest differences being for HS SBCP and MUCP of about 1000 J kg^{-1} and 500 J kg^{-1}, respectively. SBCP, MUCP, and M1CP differentiate between HS and the other two severity types for both late evening and early morning (Fig. 10; Table 4). DNCP can discriminate between all types before 05 UTC, and only between HS and NS after 05 UTC; however, relatively good separation between HS and the other two types can be seen (Fig. 10). CIN parameters were tested but no significant differences were found between the severity types. Therefore, CAPE and CIN results are analogous to those obtained considering the whole dataset.

Accepted for publication in *Weather and Forecasting*. DOI 10.1175/WAF-D-20-0137.1.

During early morning, all severity types are characterized by smaller TE3K, particularly for LS (more than 4 K less than during late evening), and smaller STHE (with the differences for HS cases between the two datasets being statistically significant). RH parameters, both at 800 hPa, 700 hPa, and between LCL and 500 hPa perform worse than what was found using the whole dataset, especially during early morning where no differences between severity types are statistically significant (Table 4). RH70 for HS environments is drier after 05 UTC than before 05 UTC, but the opposite is true for LS environments. Before 05 UTC both HS and LS RH70 mean values are similar (Table 3). LR85 and LR75 mean values are higher for HS during late evening (with the differences for LR85 for HS cases being statistically significant), whereas for LS and NS they are larger during early morning. It is not clear why the changes in lapse rates between the two periods in these layers behave differently among the severity types. Prior daytime heating may explain a warmer 850 hPa temperature, and thus greater LR85, in the late evening than in the early morning, although this impact would be smaller at 700 hPa. The nocturnal LLJ also is a source for heat and moisture that might increase lapse rates at night, so it is possible that differences in the behavior of the LLJ among the cases might explain these trends in lapse rates. Both lapse rate parameters differentiate among all severity types only during late evening, similar to the results obtained using the full sample, with large separation (Fig. 11) in the distributions between severity types. On the other hand, LR75 differentiates only between HS and NS during early morning (Table 4). The four severe composite parameters behave similarly for both time periods and similar to the previous results, with the exception that SCP does not differentiate between HS and LS for either time period. This result may be consistent with the previous finding that kinematic parameters, which play a strong role in the formation of supercells, do not differentiate either between HS and LS events. XTRN only discriminates

Accepted for publication in *Weather and Forecasting*. DOI 10.1175/WAF-D-20-0137.1.

between severe and nonsevere as well; but, contrary to the other three severe composite parameters, during early morning it shows higher mean values for severe types, with better separation between severity types than it does during the late evening (Fig. 11). Because XTRN is a function of the maximum mixing ratio and wind speed at the level of the most unstable parcel, it is likely particularly sensitive to the strength of the LLJ which supplies moisture and often has its peak intensity near the level of the most unstable parcel. The LLJ often peaks in intensity during the early morning period, which might explain the better separation of XTRN among severity types in the early morning. STP and DCP differentiate among all types for all time periods. During late evening, SCP is greater for all severity types, while STP and DCP are greater only for severe events (Table 3), and show larger separation between severity types (Fig. 12). This behavior is consistent with these composite parameters' dependence on either CAPE or steepness of low-level lapse rates, which would be greater earlier in the night than later.

For the two subsets a separate analysis of the SBL was performed as well (figure not shown). The depths of the SBL during late evening are generally shallower than those found using the whole dataset for all severity types, with almost 80% of all SBLs less than 50 hPa deep and less than 10% of the lower tropospheric temperature profiles conditionally unstable. Early morning SBL depths vary more: the majority (about 30%) are in the range 25-50 hPa, while about 18% are below 25 hPa and about 18% in the range 50-75 hPa; about 14% of all lower tropospheric temperature profiles are conditionally unstable. The increased variation happens among all severity types. Of all the parameters shown in Table 4, statistically significant differences between the values before and after 05 UTC are present only for the parameters SBCP, DNCP, STHE, and LR85 for HS only (not shown). These are all related to thermodynamics, as one would expect due to typical nocturnal cooling in the lower troposphere.

Accepted for publication in *Weather and Forecasting*. DOI 10.1175/WAF-D-20-0137.1.

It is worth noting that for HS cases there are more robust differences before and after 05 UTC than for the other two severity types.

c. Single-parameter forecast skill

In the previous discussion, it was found that only four parameters differ significantly between the first and second part of the night; therefore, the following two sections examining the skill of using the parameters to forecast severity focus on the whole dataset. Although the previous analyses are important to evaluate which forecast parameters have the best discriminatory ability between severity types, the use of thresholds and an analysis of the skill associated with them is needed to determine the usefulness of each parameter in forecasting. For this reason, HSS values were calculated to assess each parameter's suitability for predicting the severity level of nocturnal bow echoes.

The ten parameters with the highest HSS for forecasting each severity class, along with the threshold yielding that HSS value, are shown in Table 5. The four composite parameters, XTRN, SCP, STP, and DCP, are among the most highly skilled for all severity types. They have the highest HSS scores for NS environments (0.51 – 0.6), and some of the highest for LS (0.31 – 0.38) and HS (0.36 – 0.45). These results are consistent with what was found earlier, as composite parameters are functions of parameters that discriminate significantly between severe and nonsevere (shear, SRH), and at least one differing between HS and LS/NS (e.g., CAPE). In fact, considering NS cases, which do not produce severe winds at the surface, the two most skillful parameters were STP (HSS of 0.6), with a maximum threshold of 0.039 (meaning that values less than 0.039 indicate an NS event will occur), followed by SCP (0.59) and DCP (0.59),

Accepted for publication in *Weather and Forecasting*. DOI 10.1175/WAF-D-20-0137.1.

with maximum thresholds of 1.77 and 0.64 respectively. These thresholds are relatively small (Thompson et al. 2012; Lagerquist et al. 2017) and should capture the large majority of nonsevere events. The V wind component at best CAPE level (VMXP; 0.38), where best CAPE is the maximum 50 hPa mean layer CAPE or essentially a layer averaged MUCP, is the most skillful parameter for LS environments, with lower and upper thresholds of 12.82 kt and 27.39 kt respectively (i.e., LS events are forecast when VMXP is between these values). The parameters with the next highest HSS values are STP (0.35) and SCP (0.35), with higher threshold ranges than those found for NS of 0.157 – 0.905 and 1.77 – 8.0, respectively. Finally, STP (0.45) and MUCP (0.44) are the best parameters for HS events when minimum thresholds are 0.59 and 1949.4 J kg^{-1}, respectively. This result confirms both the usefulness of composite parameters in distinguishing significantly between all severity types as well as the crucial and intrinsic discriminating nature of large CAPE for HS environments.

Together with the aforementioned four composite parameters, SRH and shear parameters make up the other six most skillful parameters for NS events. A combination of kinematic and thermodynamic parameters are the others having highest skill for LS events, and mostly severe composite parameters together with CAPE parameters work best for HS environments. It is possible that CAPE parameters are skilled at differentiating between HS and LS/NS environments because stronger CAPE can lead to heavier precipitation cores and possible cold pools. These conditions can subsequently favor the creation of strong winds due to downdrafts bringing potentially cooler air down from aloft and wet-bulbing from evaporation of rain and latent cooling near the surface. Higher CAPE may also lead to stronger pressure perturbations due to the stronger updrafts, leading to stronger storm-scale jets (Adams-Selin and Johnson 2013).

Accepted for publication in *Weather and Forecasting*. DOI 10.1175/WAF-D-20-0137.1.

d. Two-parameter space analysis

Studies have shown that a multiparameter forecasting method often proves more skillful than single-parameter counterparts (e.g., Reames 2017). To assess whether combinations of parameters can provide better forecasts of severe wind potential in nocturnal bow echoes than single parameters, the forecast skill of various combinations of two parameters was analyzed in a manner similar to that used for single parameters. The combinations were created by combining each thermodynamic parameter with every kinematic and composite parameter, each kinematic parameter with every composite parameter, and the four composite parameters with each other. This yields 245 combinations. Table 6 shows the five combinations of parameters that have the best HSS scores for prediction of each severity class, along with the associated thresholds intervals. In general, multiparameter forecasting skill is greater than single-parameter forecasting skill for each severity class, with HSS differences for the best performing parameters around 20% larger (compare Table 6 to Table 5). Out of the 245 combinations of parameters (those in Table 4) analyzed, 44 have HSS values larger than the best score found for single-parameters for HS cases, with one of the two parameters being almost always a CAPE or severe composite parameter. For LS cases, 39 combinations have HSS values larger than the best score for any single parameter, and for NS, 49 do. Generally for LS and consistently for NS events, a severe composite parameter is one parameter of the combination. As one would expect for these two severity types, combining the highly discriminatory composite parameters, which account for multiple atmospheric conditions, with other kinematic or thermodynamic parameters results in more skillful combinations than combining non-composite forecasting variables only. The best

Accepted for publication in *Weather and Forecasting*. DOI 10.1175/WAF-D-20-0137.1.

five parameters for NS have the highest scores among all severity types (0.67 – 0.71), the best for HS have the second highest (0.50 – 0.53) and for LS the third highest (0.45 – 0.50).

The combination of DCP and 0-3 km SRH (SRH3) earns the highest HSS values for NS types with a score of 0.71 (Table 6), and upper thresholds of 1.3 and 243.7 $m^2 s^{-2}$ respectively. The highly concentrated area of NS environments tends to be well separated from the other two severity types and located toward smaller values of DCP and SRH3 (Fig. 13). The probability of detection (POD) of the best-performing NS combination is 0.82 with a false alarm rate (FAR) of 0.2 (not shown). This combination is likely most effective for NS environments because lower values of DCP discern unfavorable conditions for cold pool-driven wind events, and lower values of SRH3 suggest at best weak potential for cyclonic updraft rotation, and the resulting storm scale jets that can be associated with supercell thunderstorms.

The most skillful parameter combination for LS is DCP and VMXP with a score of 0.5, and threshold ranges of 0.671 – 3.35 and 11.5 – 27.5 kt. The distribution of LS events is dense and quite localized, well separated from NS types but it slightly overlaps with the broad HS group (Fig. 14). The distribution of VMXP values for LS events is similar to HS events and higher than NS, while the distribution of DCP values for LS events is lower than HS events and higher than NS events. The POD for the most skillful LS multiparameter combination is 0.56 with a FAR of 0.28 (not shown). Although it is more difficult to explain why these combinations provide the best skill for forecasting LS events since these events fall between the other two types in terms of severity, with two thresholds applied to each parameter, it appears that a strong southerly wind at the best CAPE level is important because it may help supply heat and moisture to maintain strong buoyancy while DCP was designed to indicate the potential for cold pool-driven severe surface winds.

Accepted for publication in *Weather and Forecasting*. DOI 10.1175/WAF-D-20-0137.1.

For HS events, SBCP with U6SV is the most skillful combination of forecast parameters with a score of 0.53, and lower thresholds of 657 J kg^{-1} and 29.8 kt respectively. With a POD of 0.62 and a FAR of 0.23, HS events are more broadly distributed with thinner Gaussian kernel density estimation contours, but still well separated from the other two severity groupings, especially NS ones (Fig. 15). It should be noted that the 0-6 km shear magnitude and its U component are present in all top seven combinations for HS types, indicating that, combined with CAPE parameters, they provide the most skillful forecasts for HS environments. The fact that this combination works best for HS events is not surprising when considering what parameters were found to work best in the creation of the DCP (Evans and Doswell 2001). That study did not test SBCP or U6SV, but did find that two similar parameters, MUCP and the shear magnitude in the 0-6 km layer, worked well to determine derecho environments.

4. Summary and conclusions

This work analyzes multiple meteorological variables and their ability to differentiate the severity of thunderstorm winds produced in 132 warm-season, nocturnal bow echo environments. Nocturnal bow echoes present an enhanced challenge because the typical relatively cool SBL at night reduces both the momentum of downdrafts that can lead to severe wind at the ground, and the intensity of low-level cold pools whose strong pressure gradients might drive strong winds. These cases were classified into three severity types based on the maximum severe wind or damage reports: 44 nonsevere cases (NS), 41 low-intensity severe wind cases (LS), and 47 high-intensity severe winds cases (HS). A total of 43 forecast parameters were obtained from the SPC mesoanalysis system and analyzed for both the

Accepted for publication in *Weather and Forecasting*. DOI 10.1175/WAF-D-20-0137.1.

overnight and in the subperiods of late evening and early morning. These parameters included measures of wind shear in different layers, SRH, instability, buoyancy, lapse rates, relative humidity, severe composite parameters, and other variables.

Results indicate that parameters able to discriminate between LS and NS events tend to be kinematic-based (shear, SRH) and severe composite parameters; while parameters that differentiate between HS and LS include some that are thermodynamic-based, mostly CAPE, and severe composite. Large values of buoyancy are found to be a distinctive trait of HS bow echoes, especially during late evening. In addition, DNCP is a good discriminator for all severity types only for late evening environments, but it does discriminate between severe and nonsevere in the other time periods. Similar to Kuchera and Parker (2006) who looked at nontornadic severe winds from long-lived convective windstorms, CIN variables are among the worst discriminators: this is supported by the fact that the nocturnal SBLs analyzed do not differ among the three severity types.

Midlevel dry air entrainment has often been identified as a favorable ingredient for downdraft initiation (e.g., Johns 1993), and we found drier conditions at midlevels (Coniglio et al. 2004) and significantly steeper midlevel lapse rates as severity increased. However, when separated into two nocturnal time periods, midlevel relative humidity parameters are poor discriminators for both time periods. As found by Cohen et al. (2007) for MCSs, the present study found that midlevel lapse rates were good discriminators for bow echo severity for the full sample of nocturnal events, but when examining sub-periods, they were not good discriminators for the early morning period. Severe composite parameters, especially DCP and STP, were shown to be among the most skillful discriminators between all severity types. The generally good discriminatory ability of composite parameters that take into account both the strength of

Accepted for publication in *Weather and Forecasting*. DOI 10.1175/WAF-D-20-0137.1.

shear and buoyancy is consistent with the idea that bow echoes are often a function of small-scale kinematic and thermodynamic processes, so that many single mesoanalysis parameters representing the larger near-storm environment will not work as well for the prediction of winds in bow echoes.

The two single parameters with the highest HSS values when used to forecast HS bow echoes are STP and MUCP, and for LS bow echoes VMXP together with STP and SCP are best. A multiparameter forecasting method produced improved forecast skill compared with single-parameter skill. The combination that was found to be best suited in discriminating HS bow echoes is SBCP and 0 – 6 km U shear component, while for LS bow echoes it was DCP and VMXP. Considering these two combinations, HSS values were comparable to those found in a similar study of tornado environments by Reames (2017), and should provide forecasters with improved guidance on forecasting warm-season, nocturnal bow echo severity. However, if the event is not pristine and convection may be altering the environment ahead of the bow echo, the skill of this technique may be reduced since it was developed using pristine events.

Future work should examine a larger sample of cases, and perhaps use multiple hours from each event. One of the limitations to the findings in the present study might be that they are not based on observed soundings, but on model-derived soundings adjusted using surface observations. Therefore, the dataset used in this study has somewhat lower vertical resolution compared to radiosonde data and is subject to biases and errors. Future studies should perform a similar analysis using a dataset comprising observed soundings that were taken in or near bow echo inflow regions. In addition, reanalysis data with a finer horizontal resolution could also be investigated. Furthermore, because the average soundings in the present study suggested stronger mid-level flow with the more severe events, future work should examine the components of flow

Accepted for publication in *Weather and Forecasting*. DOI 10.1175/WAF-D-20-0137.1.

relative to the bow echo orientation to explore the relationship between the magnitude of bow-perpendicular mid-level flow and intensity of the winds. Future research should assess single-parameter and multiparameter forecasting skill for the different portions of the night because threshold intervals would likely change. A separate test set of cases should be used with the thresholds and parameters found in the present study to see if the forecasting skill remains high. Finally, future studies could use the parameter results in the present study for different severity types to create environmental soundings to initialize an idealized model, such as CM1, to better understand the physical processes most important in determining how strong the winds become within nocturnal bow echoes in differing environments. A similar analysis could also be applied to multiple types of nocturnal MCSs (similar to Cohen et al. 2007) to compare and analyze differences in forecast parameters between different morphologies. Nonetheless, the results of the present study are encouraging and suggest that the intensity of winds in nocturnal bow echoes can be predicted rather well, despite the usual presence of a SBL that might suggest more difficulty in the forecasting process.

Data availability statement

The data that supports the findings of this work are available from the UCAR Image Archive browser (https://www2.mmm.ucar.edu/imagearchive) and the NOAA/NCEI website (https://www.ncdc.noaa.gov/). The SPC mesoanalysis data (Bothwell et al. 2002) for the period examined in the present study is available from the corresponding author upon request.

5. Acknowledgments

Accepted for publication in *Weather and Forecasting*. DOI 10.1175/WAF-D-20-0137.1.

This work was supported by National Science Foundation grants AGS1624947 and AGS2022888. The authors thank Daryl Herzmann and Lizzie Tirone for their help with GEMPAK and data retrieval procedures, and Israel Jirak and Kent Knopfmeier for access to the SPC mesoanalysis archive. We thank Daryl Herzmann again and Dave Flory for their assistance with Iowa State University computational resources; and Jon Thielen for his assistance with Python code. We acknowledge the importance of open source Python code and packages (Matplotlib, NumPy, MetPy), which were used extensively during this study.

6. References

Adams-Selin, R.D. and R.H. Johnson, 2010: Mesoscale surface pressure and temperature features associated with bow echoes. *Mon. Wea. Rev.*, **138**, 212–227, https://doi.org/10.1175/2009MWR2892.1.

________, and ________, 2013: Examination of gravity waves associated with the 13 March 2003 bow echo. *Mon. Wea. Rev.*, **141**, 3735–3756, https://doi.org/10.1175/MWR-D-12-00343.1.

Ashley, W. S., and T. L. Mote, 2005: Derecho hazards in the United States. *Bull. Amer. Meteor. Soc.*, **86**, 1577–1592, https://doi.org/10.1175/BAMS-86-11-1577.

Atkins, N. T., C. S. Bouchard, R. W. Przybylinski, R. J. Trapp, and G. Schmocker, 2005: Damaging surface wind mechanism within the 10 June 2003 Saint Louis bow echo during BAMEX. *Mon. Wea. Rev.*, **133**, 2275–2296, https://doi.org/10.1175/MWR2973.1.

________, and M. St. Laurent, 2009: Bow echo mesovortices. Part I: Processes that influence their damaging potential. *Mon. Wea. Rev.*, **137**, 1497–1513, https://doi.org/10.1175/2008MWR2649.1.

Bentley, M.L. and T.L. Mote, 1998: A climatology of derecho-producing mesoscale convective systems in the central and eastern United States, 1986–95. Part I: Temporal and spatial distribution. *Bull. Amer. Meteor. Soc.*, **79**, 2527–2540, https://doi.org/10.1175/1520-0477(1998)079<2527:ACODPM>2.0.CO;2.

Bernardet, L.R. and W.R. Cotton, 1998: Multiscale evolution of a derecho-producing mesoscale convective system. *Mon. Wea. Rev.*, **126**, 2991–3015, https://doi.org/10.1175/1520-0493(1998)126<2991:MEOADP>2.0.CO;2.

Blake, B. T., D. B. Parsons, K. R. Haghi, and S. G. Castleberry, 2017: The structure, evolution, and dynamics of a nocturnal convective system simulated using the WRF-ARW model. *Mon. Wea. Rev.*, **145**, 3179–3201, https://doi.org/10.1175/MWR-D-16-0360.1.

Bothwell, P. D., J. A. Hart, and R. L. Thompson, 2002: An integrated three-dimensional objective analysis scheme in use at the Storm Prediction Center. Preprints, *21st Conf. on Severe Local Storms*, San Antonio, TX, Amer. Meteor. Soc., JP3.1. [Available online at https://ams.confex.com/ams/SLS_WAF_NWP/techprogram/paper_47482.htm.]

Bryan, G. H., J. M. Fritsch, 2002: A benchmark simulation for moist nonhydrostatic numerical models. *Mon. Wea. Rev.*, **130**, 2917-2928, https://doi.org/10.1175/1520-0493(2002)130<2917:ABSFMN>2.0.CO;2.

Brooks, H. E., C. A. Doswell, and J. Cooper, 1994: On the environments of tornadic and nontornadic mesocyclones. *Wea. Forecasting*, **9**, 606–618, https://doi.org/10.1175/1520-0434(1994)009<0606:OTEOTA>2.0.CO;2.

Accepted for publication in *Weather and Forecasting*. DOI 10.1175/WAF-D-20-0137.1.

Bunkers, M. J., B. A. Klimowski, J. W. Zeitler, R. L. Thompson, and M. L. Weisman, 2000: Predicting supercell motion using a new hodograph technique. *Wea. Forecasting*, **15**, 61–79, https://doi.org/10.1175/1520-0434(2000)015<0061:PSMUAN>2.0.CO;2.

Clark, A. J., W. A. Gallus, and T. C. Chen, 2007: Comparison of the diurnal precipitation cycle in convective-resolving and non-convection-resolving mesoscale models. *Mon. Wea. Rev.*, **135**, 3456–3473, https://doi.org/10.1175/MWR3467.1.

Cohen, A.E., M.C. Coniglio, S.F. Corfidi, and S.J. Corfidi, 2007: Discrimination of mesoscale convective system environments using sounding observations. *Wea. Forecasting,* **22**, 1045–1062, https://doi.org/10.1175/WAF1040.1.

Colman, B. R., 1990: Thunderstorms above frontal surfaces in environments without positive CAPE. Part I: A climatology. *Mon. Wea. Rev.*, **118**, 1103–1121, https://doi.org/10.1175/1520-0493(1990)118<1103:TAFSIE>2.0.CO;2.

Coniglio, M. C., D. J. Stensrud, and M. B. Richman, 2004: An observational study of derecho-producing convective systems. *Wea. Forecasting*, **19**, 320–337, https://doi.org/10.1175/1520-0434(2004)019<0320:AOSODC>2.0.CO;2.

________, ________, and L. J. Wicker, 2006: Effects of upper-level shear on the structure and maintenance of strong quasi-linear mesoscale convective systems. *J. Atmos. Sci.*, **63**, 1231–1252, https://doi.org/10.1175/JAS3681.1.

________, S. F. Corfidi, and J. S. Kain, 2012: Views on applying RKW theory: An illustration using the 8 May 2009 derecho-producing convective system. *Mon. Wea. Rev.*, **140**, 1023–1043, https://doi.org/10.1175/MWR-D-11-00026.1.

Accepted for publication in *Weather and Forecasting.* DOI 10.1175/WAF-D-20-0137.1.

Corfidi, S. F., S. J. Corfidi, and D. M. Schultz, 2008: Elevated convection and castellanus: Ambiguities, significance and questions. *Wea. Forecasting* , **23**, 1280–1303, https://doi.org/10.1175/2008WAF2222118.1.

________, M.C. Coniglio, A. Cohen, and C. Mead, 2016: A proposed revision to the definition of ''Derecho.'' *Bull. Amer. Meteor. Soc.* , **97**, 935–949, https://doi.org/10.1175/BAMS-D-14-00254.1.

Craven, J. P., and H. E. Brooks, 2004: Baseline climatology of sounding derived parameters associated with deep moist convection. *Natl. Wea. Dig.* , **28**, 13–24. [Available online at http://www.nssl.noaa.gov/users/brooks/public_html/papers/cravenbrooksnwa.pdf.]

Crook, N. A., 1988: Trapping of low-level internal gravity waves. *J. Atmos. Sci.* , **45**, 1533–1541, https://doi.org/10.1175/1520-0469(1988)045<1533:TOLLIG>2.0.CO;2.

________, and M. W. Moncrieff, 1988: The effect of large–scale convergence on the generation and maintenance of deep moist convection. *J. Atmos. Sci.* , **45**, 3606–3624, https://doi.org/10.1175/1520-0469(1988)045<3606:TEOLSC>2.0.CO;2.

Davis, C. A., K. W. Manning, R. E. Carbone, S. B. Trier, and J. D. Tuttle, 2003: Coherence of warm-season continental rainfall in numerical weather prediction models. *Mon. Wea. Rev.*, **131**, 2667–2679, https://doi.org/10.1175/1520-0493(2003)131<2667:COWCRI>2.0.CO;2.

________, N. Atkins, D. Bartels, L. Bosart, M. Coniglio, G. Bryan, W. Cotton, D. Dowell, B. Jewett, R. Johns, D. Jorgensen, J. Knievel, K. Knupp, W. Lee, G. McFarquhar, J. Moore, R. Przybylinski, R. Rauber, B. Smull, R. Trapp, S. Trier, R. Wakimoto, M. Weisman, and C. Ziegler, 2004: The bow echo and MCV experiment: Observations and

Accepted for publication in *Weather and Forecasting*. DOI 10.1175/WAF-D-20-0137.1.

opportunities. *Bull. Amer. Meteor. Soc.,* **85**, 1075–1094, https://doi.org/10.1175/BAMS-85-8-1075.

desJardins, M. L., K. F. Brill, and S. S. Schotz, 1991: Use of GEMPAK on UNIX workstations. *Proc. Seventh Int. Conf. on Interactive Information and Processing Systems for Meteorology, Oceanography, and Hydrology,* New Orleans, LA, Amer. Meteor. Soc., 449–453. Google Scholar

Doswell, C.A., III, and J.S. Evans, 2003: Proximity sounding analysis for derechos and supercells: An assessment of similarities and differences. *Atmos. Res.*, **67–68**, 117–133, https://doi.org/10.1016/S0169-8095(03)00047-4.

Edwards, R., J. T. Allen, and G. W. Carbin, 2018: Reliability and Climatological Impacts of Convective Wind Estimations. *J. Appl. Meteor. Climatol.*, **57**, 1825–1845, https://doi.org/10.1175/JAMC-D-17-0306.1.

Evans, J.S. and C.A. Doswell III, 2001: Examination of derecho environments using proximity soundings. *Wea. Forecasting,* **16**, 329–342, https://doi.org/10.1175/1520-0434(2001)016<0329:EODEUP>2.0.CO;2.

French, A. J., and M. D. Parker, 2010: The response of simulated nocturnal convective systems to a developing low-level jet. *J. Atmos. Sci.*, **67**, 3384–3408, https://doi.org/10.1175/2010JAS3329.1.

Fujita, T. T., 1978: Manual of downburst identification for project NIMROD. Satellite and Mesometeorology Research Paper No 156, Department of Geophysical Sciences, University of Chicago, 104 pp. [NTIS PB-286048] Google Books

________ and R. M. Wakimoto, 1981: Five scales of airflow associated with a series of downbursts of 16 July 1980. *Mon. Wea. Rev.*, **109**, 1438–1456,

Accepted for publication in *Weather and Forecasting.* DOI 10.1175/WAF-D-20-0137.1.

https://doi.org/10.1175/1520-0493(1981)109<1438:FSOAAW>2.0.CO;2.

Geerts, B., and Coauthors, 2017: The 2015 Plains Elevated Convection at Night field project. *Bull. Amer. Meteor. Soc.* , **98**, 767–786, https://doi.org/10.1175/BAMS-D-15-00257.1.

Guastini, C.T. and L.F. Bosart, 2016: Analysis of a progressive derecho climatology and associated formation environments. *Mon. Wea. Rev.,* **144**, 1363–1382, https://doi.org/10.1175/MWR-D-15-0256.1.

Haghi, K. R., D. B. Parsons, and A. Shapiro, 2017: Bores observed during IHOP_2002: The relationship of bores to the nocturnal environment. *Mon. Wea. Rev.* , **145**, 3929–3946, https://doi.org/10.1175/MWR-D-16-0415.1.

Hampshire, N. L., R. M. Mosier, T.M. Ryan, and D.E. Cavanaugh, 2017: Relationship of low-level instability and tornado damage rating based on observed soundings. *J. Operational Meteor.* , **6**, 1-12, https://doi.org/10.15191/nwajom.2018.0601.

Heidke, P., 1926: Calculation of the success and goodness of strong wind forecasts in the storm warning service. *Geogr. Ann.* , **8**, 301–349. Google Scholar

Hiris, Z. A. and W. A. Gallus, Jr., 2020: Factors Contributing to Upscale Convective Growth in the Central Great Plains of the United States. *Mon. Wea. Rev* . (submitted).

Hitchcock, S. M., R. S. Schumacher, G. R. Herman, M. C. Coniglio, M. D. Parker, and C. L. Ziegler, 2019: Evolution of pre- and postconvective environment profiles from mesoscale convective systems during PECAN. *Mon. Wea. Rev.* , **147**, 2329–2354, https://doi.org/10.1175/MWR-D-18-0231.1.

Horgan, K.L., D.M. Schultz, J.E. Hales, S.F. Corfidi, and R.H. Johns, 2007: A Five-Year Climatology of Elevated Severe Convective Storms in the United States East of the

Accepted for publication in *Weather and Forecasting*. DOI 10.1175/WAF-D-20-0137.1.

Rocky Mountains. *Wea. Forecasting,* **22**, 1031–1044, https://doi.org/10.1175/WAF1032.1.

James, R.P., P.M. Markowski, and J.M. Fritsch, 2006: Bow echo sensitivity to ambient moisture and cold pool strength. *Mon. Wea. Rev.,* **134**, 950–964, https://doi.org/10.1175/MWR3109.1.

Johns, R.H., and W.D. Hirt, 1987: Derechos: Widespread convectively induced windstorms. *Wea. Forecasting,* **2**, 32–49, https://doi.org/10.1175/1520-0434(1987)002<0032:DWCIW>2.0.CO;2.

________, and C. A. Doswell III, 1992: Severe local storms forecasting. *Wea. Forecasting*, **7**, 588–612, https://doi.org/10.1175/1520-0434(1992)007<0588:SLSF>2.0.CO;2.

________, 1993: Meteorological conditions associated with bow echo development in convective storms. *Wea. Forecasting,* **8**, 294–299, https://doi.org/10.1175/1520-0434(1993)008<0294:MCAWBE>2.0.CO;2.

Koch, S.E., W. Feltz, F. Fabry, M. Pagowski, B. Geerts, K. M. Bedka, D. O. Miller, and J. W. Wilson, 2008: Turbulent mixing processes in atmospheric bores and solitary waves deduced from profiling systems and numerical simulation. *Mon. Wea. Rev.*, **136**, 1373–1400, https://doi.org/10.1175/2007MWR2252.1.

Kuchera, E.L. and M.D. Parker, 2006: Severe convective wind environments. *Wea. Forecasting,* **21**, 595–612, https://doi.org/10.1175/WAF931.1.

Lagerquist, R., A. McGovern, and T. Smith, 2017: Machine learning for real-time prediction of damaging straight-line convective wind. *Wea. Forecasting*, **32**, 2175–2193, https://doi.org/10.1175/WAF-D-17-0038.1.

Marsham, J. H., K. A. Browning, J. C. Nicol, D. J. Parker, E. G. Norton, A. M. Blyth, U.

Accepted for publication in *Weather and Forecasting*. DOI 10.1175/WAF-D-20-0137.1.

Corsmeier, and F. M. Perry, 2010: Multi-sensor observations of a wave beneath an impacting rear-inflow jet in an elevated mesoscale convective system. *Quart. J. Roy. Meteor. Soc.*, **136**, 1788–1812, https://doi.org/10.1002/qj.669.

________, S. B. Trier, T. M. Weckwerth, and J. W. Wilson, 2011: Observations of elevated convection initiation leading to a surface based squall line during 13 June IHOP_2002. *Mon. Wea. Rev.* , **139**, 247–271, https://doi.org/10.1175/2010MWR3422.1.

Mendenhall, W. M., and T. L. Sincich, 2007: *Statistics for Engineering and the Sciences*. CRC Press, 1072 pp. Google Scholar

Parker, M. D., 2008: Response of simulated squall lines to low-level cooling. *J. Atmos. Sci.* , **65**, 1323–1341, https://doi.org/10.1175/2007JAS2507.1.

________, B.S. Borchardt, R.L. Miller, and C.L. Ziegler, 2020: Simulated evolution and severe wind production by the 25–26 June 2015 nocturnal MCS from PECAN. *Mon. Wea. Rev.,* **148**, 183–209, https://doi.org/10.1175/MWR-D-19-0072.1.

Parsons, D. B., K. R. Haghi, K. T. Halbert, B. Elmer, and J. Wang, 2019: The potential role of atmospheric bores and gravity waves in the initiation and maintenance of nocturnal convection over the southern great plains. *J. Atmos. Sci* ., **76**, 43–68, https://doi.org/10.1175/JAS-D-17-0172.1.

Peters, J. M., and R. S. Schumacher, 2016: Dynamics governing a simulated mesoscale convective system with a training convective line. *J. Atmos. Sci.* , **73**, 2643–2664, https://doi.org/10.1175/JAS-D-15-0199.1.

Przybylinski, R., 1995: The bow echo: Observations, numerical simulations, and severe weather detection methods. *Wea. Forecasting* , **10**, 203–218, https://doi.org/10.1175/1520-0434(1995)010<0203:TBEONS>2.0.CO;2.

Accepted for publication in *Weather and Forecasting.* DOI 10.1175/WAF-D-20-0137.1.

Reames, L. J., 2017: Diurnal variations in severe weather forecast parameters of Rapid Update Cycle-2 tornado proximity environments. *Wea. Forecast.* , **32**, 743–761, https://doi.org/10.1175/WAF-D-16-0029.1.

Rotunno, R., J. B. Klemp, and M. L. Weisman, 1988: A theory for strong, long-lived squall lines. *J. Atmos. Sci.* , **45**, 463–485, https://doi.org/10.1175/1520-0469(1988)045<0463:ATFSLL>2.0.CO;2.

Schultz, D. M., P. N. Schumacher, and C. A. Doswell III, 2000: The intricacies of instabilities. *Mon. Wea. Rev.* , **128**, 4143–4148, https://doi.org/10.1175/1520-0493(2000)129<4143:TIOI>2.0.CO;2.

Schumacher, R. S., and R. H. Johnson, 2009: Quasi-stationary, extreme-rain-producing convective systems associated with midlevel cyclonic circulations. *Wea. Forecasting* , **24**, 555–574, https://doi.org/10.1175/2008WAF2222173.1.

Scott, DW., 2015: *Multivariate density estimation: theory, practice, and visualization*. 2nd edition, the first is from 1992. New Jersey: Wiley. Google Scholar

Smith, B.T., R.L. Thompson, J.S. Grams, C. Broyles, and H.E. Brooks, 2012: Convective modes for significant severe thunderstorms in the contiguous United States. Part I: Storm classification and climatology. *Wea. Forecasting,* **27**, 1114–1135, https://doi.org/10.1175/WAF-D-11-00115.1.

Stull, R. B., 1988: *An Introduction to Boundary Layer Meteorology* . Kluwer Academic, 666 pp. Google Scholar

Thompson, R. L., R. Edwards, J. A. Hart, K. L. Elmore, and P. Markowski, 2003: Close proximity soundings within supercell environments obtained from the Rapid Update

Accepted for publication in *Weather and Forecasting*. DOI 10.1175/WAF-D-20-0137.1.

Cycle. *Wea. Forecasting*, **18**, 1243–1261, https://doi.org/10.1175/1520-0434(2003)018<1243:CPSWSE>2.0.CO;2.

________, ________, and C. M. Mead, 2004: An update to the supercell composite and significant tornado parameters. Preprints, 22nd Conf. Severe Local Storms, Hyannis, MA, Amer. Meteor. Soc., P8.1. [Available online at https://ams.confex.com/ams/11aram22sls/techprogram/paper_82100.htm.]

________, B. T. Smith, J. S. Grams, A. R. Dean, and C. Broyles, 2012: Convective modes for significant severe thunderstorms in the contiguous United States. Part II: Supercell and QLCS tornado environments. *Wea. Forecasting*, **27**, 1136–1154, https://doi.org/10.1175/WAF-D-11-00116.1.

Wakimoto, R.M., H.V. Murphey, A. Nester, D.P. Jorgensen, and N.T. Atkins, 2006: High winds generated by bow echoes. Part I: Overview of the Omaha bow echo 5 July 2003 storm during BAMEX. *Mon. Wea. Rev.*, **134**, 2793–2812, https://doi.org/10.1175/MWR3215.1.

Weckwerth, T.M., J. Hanesiak, J.W. Wilson, S.B. Trier, S.K. Degelia, W.A. Gallus, R.D. Roberts, and X. Wang, 2019: Nocturnal convection initiation during PECAN 2015. *Bull. Amer. Meteor. Soc.*, **100**, 2223–2239, https://doi.org/10.1175/BAMS-D-18-0299.1.

Weisman, M. L., 1993: The genesis of severe, long-lived bow echoes. *J. Atmos. Sci.*, **50**, 645–670, https://doi.org/10.1175/1520-0469(1993)050<0645:TGOSLL>2.0.CO;2.

________, and R.J. Trapp, 2003: Low-level mesovortices within squall lines and bow echoes. Part I: Overview and dependence on environmental shear. *Mon. Wea. Rev.*, **131**, 2779–2803, https://doi.org/10.1175/1520-0493(2003)131<2779:LMWSLA>2.0.CO;2.

Accepted for publication in *Weather and Forecasting*. DOI 10.1175/WAF-D-20-0137.1.

________, and R. Rotunno, 2004: “A theory for strong long-lived squall lines” revisited. *J. Atmos. Sci.*, **61**, 361–382, https://doi.org/10.1175/1520-0469(2004)061<0361:ATFSLS>2.0.CO;2.

________, C. Davis, W. Wang, K. W. Manning, and J. B. Klemp, 2008: Experiences with 0–36-h explicit convective forecasts with the WRF-ARW model. *Wea. Forecasting*, **23**, 407–437, https://doi.org/10.1175/2007WAF2007005.1.

Wheatley, D.M., R.J. Trapp, and N.T. Atkins, 2006: Radar and damage analysis of severe bow echoes observed during BAMEX. *Mon. Wea. Rev.*, **134**, 791–806, https://doi.org/10.1175/MWR3100.1.

Wilks, D. S., 2011: *Statistical Methods in the Atmospheric Sciences*. 3rd ed. International Geophysics Series, Vol. 100, Academic Press, 704 pp. Google Scholar

Wilson, J. W., and R. D. Roberts, 2006: Summary of convective storm initiation and evolution during IHOP: Observational and modeling perspective. *Mon. Wea. Rev.*, **134**, 23–47, https://doi.org/10.1175/MWR3069.1.

Accepted for publication in *Weather and Forecasting*. DOI 10.1175/WAF-D-20-0137.1.

Tables

Table 1: Name, description, and mean values of the parameters examined (the highest absolute values for each parameter are in bold), categorized as kinematic, thermodynamic, and composite.

Name	Description	NS	LS	HS
	Kinematic parameters			
S1MG (kt)	0-1 km shear magnitude	16.0	**25.4**	25.3
SRH1 (m^2 s^{-2})	0-1 km storm relative helicity	102	**215**	206
SRH3 (m^2 s^{-2})	0-3 km storm relative helicity	163	**307**	295
U3SV (kt)	0-3 km U shear component	15.19	**23.71**	21.94
V3SV (kt)	0-3 km V shear component	3.08	7.70	**12.6**
UPMW (kt)	0-6 km pressure-weighted U component	8.73	**14.2**	12.4
VPMW (kt)	0-6 km pressure-weighted V component	5.90	13.6	**14.4**
S6MG (kt)	0-6 km shear magnitude	27.4	36.9	**41.1**
U6SV (kt)	0-6 km U shear component	22.4	31.6	**36.2**
V6SV (kt)	0-6 km V shear component	2.90	5.99	**8.91**
U8SV (kt)	0-8 km pressure-weighted U component wind	26.4	35.0	**39.8**
V8SV (kt)	0-8 km pressure-weighted V component wind	4.94	5.32	**5.33**
VKLC (ub s^{-1})	Average kinematic vert vel (MUPL-LCL)	-0.00253	-0.00490	**-0.00674**
UWND (kt)	Surface U wind component	-0.933	-1.42	**-1.67**
VWND (kt)	Surface V wind component	0.139	**1.38**	0.902
UEIL (kt)	U comp top of effective inflow layer	8.04	**15.1**	12.5
UMXP (kt)	U wind component at best CAPE level	5.77	**8.07**	3.74
VEIL (kt)	V comp top of effective inflow layer	5.76	13.6	**14.1**
VMXP (kt)	V wind component at best CAPE level	9.74	**20.4**	17.6
	Thermodynamic parameters			
M1CP (J kg^{-1})	100 hPa mean mixed CAPE	712	949	**1605**
M1CN (J kg^{-1})	100 hPa mean mixed CIN	**-150**	-140	-141
3KRH (%)	3 km average relative humidity	**74.0**	71.1	68.7
RHC5 (%)	Average relative humidity LCL to 500 hPa	**67.0**	65.2	59.5
RHLC (%)	Average relative humidity LCL to LFC	**77.4**	75.4	73.3
ASRH (%)	Average sub-cloud humidity	**75.6**	74.9	75.4
DNCP (J kg^{-1})	Downdraft CAPE	746	878	**1025**
LR75 (C km^{-1})	Lapse Rate from 700 to 500 hPa	6.57	6.89	**7.27**
LR85 (C km^{-1})	Lapse Rate from 850 to 500 hPa	6.21	6.47	**6.62**
LLLR (C km^{-1})	Lower-level lapse rate surface to 3km AGL	5.06	5.29	**5.33**
TE3K (K)	Max Theta-e difference in lowest 3 km	11.7	14.4	**19.3**
MXMX (g kg^{-1})	Maximum mixing ratio	12.1	12.7	**13.9**
MUCP (J kg^{-1})	Most Unstable CAPE	1261	1564	**2363**
MUCN (J kg^{-1})	Most Unstable CIN	-68.1	**-71.4**	-54.8
RH70 (%)	Relative humidity 700 hPa	**71.7**	68.0	61.1
RH80 (%)	Relative humidity 800 hPa	75.9	**76.6**	72.2
SLCH (m)	Sfc based LCL height	488	532	**608**
STHE (C)	Surface equivalent potential temperature	338	340	**345**
SBCP (J kg^{-1})	Surface-based CAPE	652	872	**1518**
SBCN (J kg^{-1})	Surface-based CIN	-235	**-244**	-232
	Composite parameters			
XTRN (g kt kg^{-1})	(MXMX) * (wind speed at MUPL)	196	330	**358**
DCP (numeric)	Derecho Composite Parameter	0.676	1.57	**3.48**

Accepted for publication in *Weather and Forecasting*. DOI 10.1175/WAF-D-20-0137.1.

STP (numeric)	Sig Tornado Parameter-Fixed Layer	0.159	0.467	**1.11**
SCP (numeric)	Supercell Composite Parameter-Effective Layer	1.37	5.32	**8.55**

Accepted for publication in *Weather and Forecasting.* DOI 10.1175/WAF-D-20-0137.1.

Table 2: Results from bootstrapped paired t-tests (given in %) for all comparisons between two severity types. P-values greater than 5% are not shown. Parameters for which no test was statistically significant for any of the three pairs are not shown.

Parameter	**p (%) LS - NS**	**p (%) HS - NS**	**p (%) HS - LS**
VWND (kt)	2.45	—	—
SRH1 (m^2 s^{-2})	≤0.02	≤0.02	—
S1MG (kt)	≤0.02	≤0.02	—
SRH3 (m^2 s^{-2})	≤0.02	≤0.02	—
U3SV (kt)	≤0.02	0.32	—
V3SV (kt)	—	0.03	—
S6MG (kt)	0.06	≤0.02	—
U6SV (kt)	0.11	≤0.02	—
UPMW (kt)	0.27	2.96	—
VPMW (kt)	≤0.02	≤0.02	—
U8SV (kt)	0.32	≤0.02	—
VMXP (kt)	≤0.02	0.32	—
UEIL (kt)	0.45	—	—
VEIL (kt)	0.03	0.55	—
VKLC (ub s^{-1})	0.27	≤0.02	—
SBCP (J kg^{-1})	—	≤0.02	0.07
MUCP (J kg^{-1})	—	≤0.02	≤0.02
M1CP (J kg^{-1})	—	≤0.02	0.08
DNCP (J kg^{-1})	3.16	≤0.02	2.95
STHE (C)	—	0.44	1.20
TE3K (K)	4.02	1.14	—
RH80 (%)	—	—	3.29
RH70 (%)	—	3.88	1.57
RHC5 (%)	—	3.29	—
LR85 (C km^{-1})	3.17	0.05	—
LR75 (C km^{-1})	4.92	≤0.02	2.62
MXMX (g kg^{-1})	—	0.29	3.31
XTRN (g kt kg^{-1})	≤0.02	≤0.02	—
SCP (numeric)	0.04	≤0.02	1.81
STP (numeric)	0.22	≤0.02	0.04
DCP (numeric)	≤0.02	≤0.02	0.13

Accepted for publication in *Weather and Forecasting.* DOI 10.1175/WAF-D-20-0137.1.

Table 3: Mean values for late evening (before 05 UTC) and early morning (after 05 UTC) for parameters found to differ significantly between at least two severity types for at least one time period. Parameters for which no differences between any of the three severity types were statistically significant for either time period are not shown. Highest absolute values for each parameter are in bold.

	Before 5Z			After 5Z		
Parameter	**NS**	**LS**	**HS**	**NS**	**LS**	**HS**
SRH1 (m^2 s^{-2})	85.7	**204**	191	112	**229**	220
S1MG (kt)	15.0	24.5	**24.7**	16.7	**26.7**	25.9
SRH3 (m^2 s^{-2})	169	**306**	282	160	**309**	308
U3SV (kt)	16.0	**22.8**	21.5	14.6	**25.0**	22.4
V3SV (kt)	5.62	8.27	**10.34**	1.32	6.88	**14.82**
S6MG (kt)	25.8	38.9	**40.2**	28.6	34.2	**42.0**
U6SV (kt)	18.7	32.2	**35.8**	25.0	30.8	**36.7**
UPMW (kt)	7.32	**13.33**	11.87	9.71	**15.38**	12.91
VPMW (kt)	7.13	**14.00**	13.89	5.05	13.01	**14.90**
U8SV (kt)	22.3	34.5	**38.6**	29.2	35.7	**40.9**
VMXP (kt)	11.4	**20.3**	15.6	8.57	**20.6**	19.5
VEIL (kt)	7.00	12.7	**14.6**	4.97	**15.0**	13.4
VKLC (ub s^{-1})	-0.00253	-0.00438	**-0.00712**	-0.00253	-0.00563	**-0.00638**
SBCP (J kg^{-1})	755	1071	**2005**	580	591	**1052**
MUCP (J kg^{-1})	1250	1661	**2617**	1269	1429	**2119**
M1CP (J kg^{-1})	744	1058	**1838**	689	796	**1380**
DNCP (J kg^{-1})	776	909	**1133**	726	836	**922**
STHE (C)	342	341	**348**	335	339	**342**
TE3K (K)	13.6	16.0	**20.9**	10.6	11.7	**17.5**
RH70 (%)	**70.3**	64.9	63.5	72.6	**73.2**	58.4
RHC5 (%)	**68.4**	62.0	57.3	66.1	**69.6**	61.6
LR85 (C km^{-1})	6.06	6.46	**6.89**	6.30	**6.48**	6.36
LR75 (C km^{-1})	6.39	6.80	**7.36**	6.70	7.01	**7.18**
MXMX (g kg^{-1})	12.7	12.8	**13.8**	11.7	12.6	**13.9**
XTRN (g kt kg^{-1})	203	324	**329**	191	339	**385**
SCP (numeric)	1.58	5.83	**9.70**	1.22	4.60	**7.45**
STP (numeric)	0.0778	0.556	**1.32**	0.215	0.342	**0.906**
DCP (numeric)	0.524	1.75	**3.96**	0.782	1.32	**3.03**

Accepted for publication in *Weather and Forecasting.* DOI 10.1175/WAF-D-20-0137.1.

Table 4: As in Table 2, but for all events grouped between before and after 05 UTC.

	Before 05 UTC - p (%)			After 05 UTC - p (%)		
Parameter	**LS - NS**	**HS - NS**	**HS - LS**	**LS - NS**	**HS - NS**	**HS - LS**
SRH1 (m^2 s^{-2})	≤0.02	1.08	—	0.31	0.22	—
S1MG (kt)	0.03	0.39	—	0.03	0.07	—
SRH3 (m^2 s^{-2})	0.23	3.12	—	0.03	0.02	—
U3SV (kt)	—	—	—	0.07	0.83	—
V3SV (kt)	—	—	—	—	≤0.02	—
S6MG (kt)	0.09	0.06	—	—	≤0.02	—
U6SV (kt)	0.11	0.08	—	—	0.14	—
UPMW (kt)	3.07	—	—	4.69	—	—
VPMW (kt)	2.22	—	—	0.34	0.36	—
U8SV (kt)	0.48	0.10	—	—	0.26	—
VMXP (kt)	0.41	—	—	0.02	0.26	—
VEIL (kt)	—	—	—	4.42	2.31	—
VKLC (ub s^{-1})	—	0.07	3.90	2.54	1.37	—
SBCP (J kg^{-1})	—	≤0.02	0.16	—	0.52	3.90
MUCP (J kg^{-1})	—	≤0.02	0.38	—	0.25	1.03
M1CP (J kg^{-1})	—	0.05	1.28	—	0.20	4.16
DNCP (J kg^{-1})	3.07	0.02	0.60	—	3.77	—
STHE (C)	—	—	1.20	—	—	—
TE3K (K)	—	—	4.92	—	0.07	3.90
RH70 (%)	2.22	—	—	—	—	—
RHC5 (%)	—	2.23	—	—	—	—
LR85 (C km^{-1})	4.46	≤0.02	1.20	—	—	—
LR75 (C km^{-1})	4.51	0.03	3.33	—	2.31	—
MXMX (g kg^{-1})	—	—	—	—	0.83	—
XTRN (g kt kg^{-1})	0.05	0.63	—	0.02	≤0.02	—
SCP (numeric)	≤0.02	≤0.02	—	0.10	≤0.02	—
STP (numeric)	≤0.02	≤0.02	0.78	0.79	≤0.02	0.64
DCP (numeric)	≤0.02	≤0.02	0.22	3.47	≤0.02	3.66

Accepted for publication in *Weather and Forecasting*. DOI 10.1175/WAF-D-20-0137.1.

Table 5**:** The ten highest HSS values and their corresponding optimal threshold range for all single-parameter Heidke skill score tests for each severity type.

Severity	**Parameter**	**Threshold Range**	**HSS**
NS	STP (numeric)	< 0.039	0.6
	SCP (numeric)	< 1.77	0.59
	DCP (numeric)	< 0.64	0.59
	XTRN (g kt kg^{-1})	< 260.18	0.51
	SRH3 (m^{2} s^{-2})	< 167.09	0.48
	S6MG (kt)	< 33.21	0.44
	S1MG (kt)	< 14.77	0.43
	SRH1 (m^{2} s^{-2})	< 148.75	0.42
	U6SV (kt)	< 24.36	0.42
	VMXP (kt)	< 12.82	0.39
Severity	**Parameter**	**Threshold Range**	**HSS**
LS	VMXP (kt)	12.82 – 27.39	0.38
	STP (numeric)	0.157 – 0.905	0.35
	SCP (numeric)	1.77 – 8.0	0.35
	XTRN (g kt kg^{-1})	242.67 – 382.77	0.33
	U3SV (kt)	22.50 – 35.33	0.32
	DCP (numeric)	0.64 – 3.18	0.31
	VPMW (kt)	9.39 – 25.30	0.3
	SRH1 (m^{2} s^{-2})	148.75 – 495.23	0.29
	STHE (C)	324.43 – 335.79	0.28
	M1CP (J kg^{-1})	122.98 – 614.88	0.27
Severity	**Parameter**	**Threshold Range**	**HSS**
HS	STP (numeric)	> 0.59	0.45
	MUCP (J kg^{-1})	> 1949.4	0.44
	DCP (numeric)	> 1.78	0.42
	SCP (numeric)	> 3.64	0.42
	M1CP (J kg^{-1})	> 1147.8	0.42
	SBCP (J kg^{-1})	> 657.35	0.39
	TE3K (K)	> 22.85	0.37
	XTRN (g kt kg^{-1})	> 289.37	0.36
	U6SV (kt)	> 35.14	0.35
	DNCP (J kg^{-1})	> 1162.6	0.33

Accepted for publication in *Weather and Forecasting*. DOI 10.1175/WAF-D-20-0137.1.

Table 6: The five highest HSS values and their corresponding optimal threshold ranges for all two-parameter Heidke skill score tests for each severity type.

Severity	**Combination**	**$x_{opt,1}$ Range**	**$x_{opt,2}$ Range**	**HSS**
	DCP + SRH3	< 1.27	< 244 (m^2 s^{-2})	0.71
	DCP + U3SV	< 0.892	< 21.9 (kt)	0.68
NS	SCP + XTRN	< 1.77	< 289 (g kt kg^{-1})	0.67
	DCP + S6MG	< 0.892	< 35.7 (kt)	0.67
	STP + SCP	< 0.157	< 1.77	0.67
Severity	**Combination**	**$x_{opt,1}$ Range**	**$x_{opt,2}$ Range**	**HSS**
	DCP + VMXP	0.671 – 3.35	11.5 – 27.5 (kt)	0.50
	SCP + VMXP	1.54 – 11.4	11.5 – 27.5 (kt)	0.46
LS	XTRN + SCP	252 – 467 (g kt kg^{-1})	1.54 – 8.10	0.46
	M1CP + VMXP	216 – 2373 (J kg^{-1})	11.5 – 27.5 (kt)	0.45
	SCP + DCP	1.54 – 11.4	0.671 – 3.35	0.45
Severity	**Combination**	**$x_{opt,1}$ Range**	**$x_{opt,2}$ Range**	**HSS**
	SBCP + U6SV	> 657 (J kg^{-1})	> 29.8 (kt)	0.53
	SBCP + S6MG	> 657 (J kg^{-1})	> 25.6 (kt)	0.53
HS	M1CP + S6MG	> 738 (J kg^{-1})	> 24.4 (kt)	0.52
	MUCP + S6MG	> 1401 (J kg^{-1})	> 24.4 (kt)	0.51
	STHE + U6SV	> 336 (° C)	> 29.8 (kt)	0.50

Accepted for publication in *Weather and Forecasting*. DOI 10.1175/WAF-D-20-0137.1.

List of Figures

Fig. 1. Location of all the high-intensity severe (HS; orange), low-intensity severe (LS; green), and nonsevere (NS; blue) nocturnal bow echo events for the period 2010 – 18 used in the present study.

Fig. 2. Box-and-whiskers plots for all cases of SRH1 and SHR3 (values plotted along the left axis), and S1MG, U3SV, V3SV, U6SV, S6MG, and U8SV (values plotted along the right axis). Each color-filled box represents the results for NS (blue), LS (green), and HS (orange). The whiskers span the interval from the 10th to 90th percentiles and the boxes enclose the 25th to 75th percentiles. Outliers, or points outside the whiskers, are not plotted.

Fig. 3. As in Fig. 1, but for SBCP, MUCP, M1CP, DNCP (values plotted along the left axis), and SBCN, MUCN, and M1CN (values plotted along the right axis).

Fig. 4. As in Fig. 1, but for RH80, RH70, and RHC5 (values plotted along the left axis), and LR85 and LR75 (values plotted along the right axis).

Fig. 5. As in Fig. 1, but for SCP (values plotted along the left axis), and STP and DCP (values plotted along the right axis).

Fig. 6. Skew T-Log*p* sounding diagrams for (a) NS, (b) LS, and (c) HS environments, created by averaging all cases for each type. Temperature (red), dewpoint (green), and most

Accepted for publication in *Weather and Forecasting*. DOI 10.1175/WAF-D-20-0137.1.

unstable parcel (black) profiles are plotted, along with winds on the right side, dry adiabats (dashed red), moist adiabats (dashed blue), and constant mixing ratio lines (dashed green). MUCAPE and MUCIN are indicated by the shaded red and blue areas, respectively.

Fig. 7. Frequency of occurrence (in %) of SBLs of specified depth (in hPa) for all severity categories. For each interval the largest depth is inclusive, while the lowest is exclusive. Percentages are calculated with respect to the total number of NS (blue), LS (green), and HS (orange) events, and the total sum of all cases (yellow), respectively.

Fig. 8. Nocturnal distribution of NS (blue), LS (green), and HS (orange) events by hour of mesoanalysis data used.

Fig. 9. As in Fig. 2, but for SRH1 and SHR3 (values plotted along the left axis), and S1MG, U3SV, S6MG, and U8SV (values plotted along the right axis) for (a) late evening and (b) early morning.

Fig. 10. As in Fig. 3, but only for SBCP, MUCP, M1CP, and DNCP for (a) late evening and (b) early morning.

Fig. 11. As in Fig. 4, but only for XTRN (values plotted along the left axis), and LR85 and LR75 (values plotted along the right axis), for (a) late evening and (b) early morning.

Accepted for publication in *Weather and Forecasting*. DOI 10.1175/WAF-D-20-0137.1.

Fig. 12. As in Fig. 5, but for (a) late evening and (b) early morning.

Fig. 13. Scatter plot of DCP vs SRH3 with GDKE (Gaussian kernel density estimation) contours overlaid for all severity types (NS in blue, LS in green, and HS in orange). The three GKDE contours for each severity type encompass the top 10% (innermost contour), top 25%, and top 75% (outermost contour) densest points. The vertical and horizontal blue lines indicate the two optimal thresholds associated with the highest HSS values for prediction of NS events for DCP and SRH3, respectively.

Fig. 14. As in Fig. 13, but for DCP vs VMXP. The vertical and horizontal lines indicate the two optimal lower and upper thresholds associated with the highest HSS values for prediction of LS events for DCP and VMXP, respectively.

Fig. 15. As in Fig. 13, but for SBCP vs U6SV. The vertical and horizontal lines indicate the two optimal thresholds associated with the highest HSS values for prediction of HS events for SBCP and U6SV, respectively.

Accepted for publication in *Weather and Forecasting*. DOI 10.1175/WAF-D-20-0137.1.

Figures

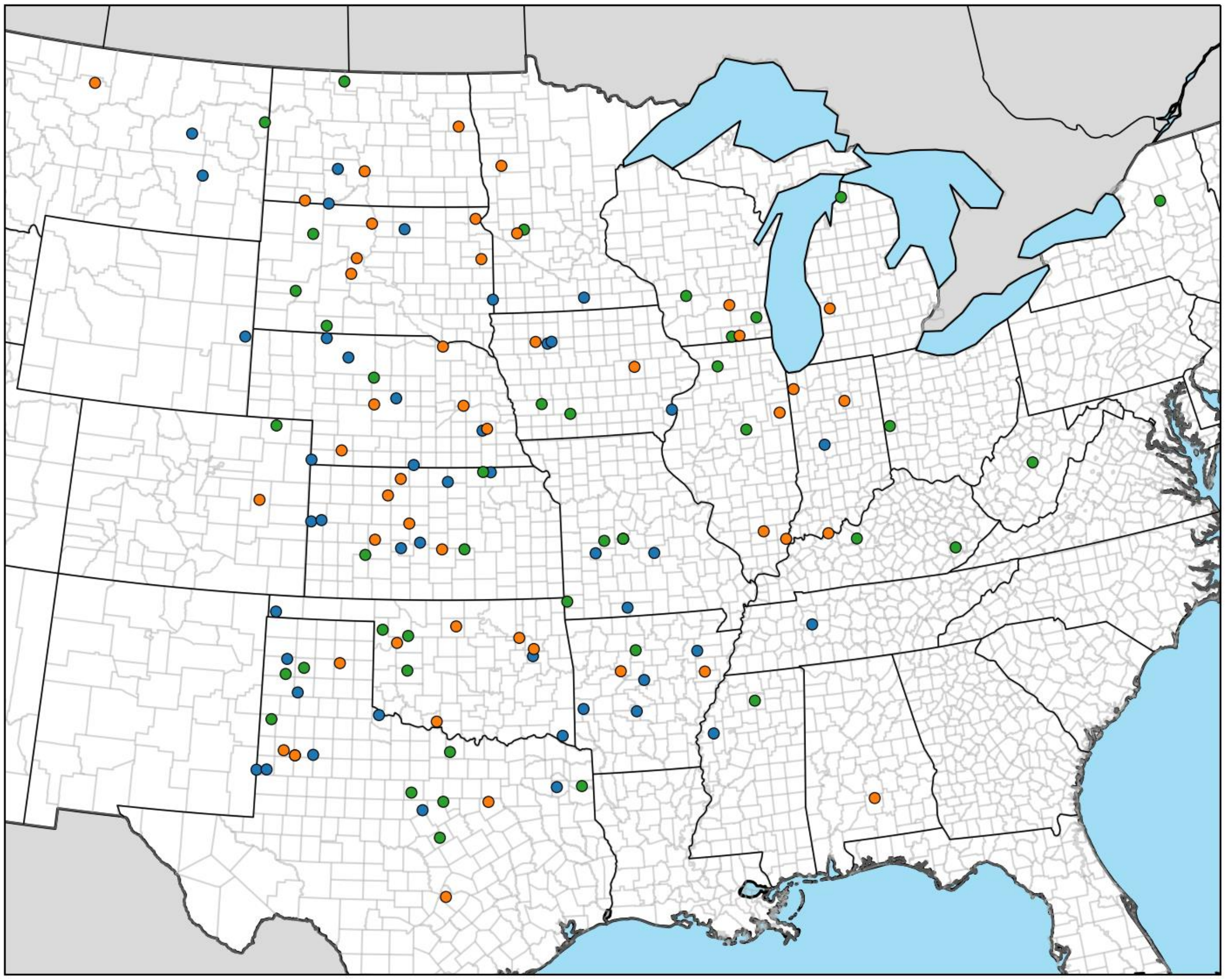

Figure 1: Location of all the high-intensity severe (HS; orange), low-intensity severe (LS; green), and nonsevere (NS; blue) nocturnal bow echo events for the period 2010 – 2018 used in the present study. The plotted points indicate the locations of the storm reports used for severe cases and the points closest to the apex of the bow for nonsevere.

Accepted for publication in *Weather and Forecasting*. DOI 10.1175/WAF-D-20-0137.1.

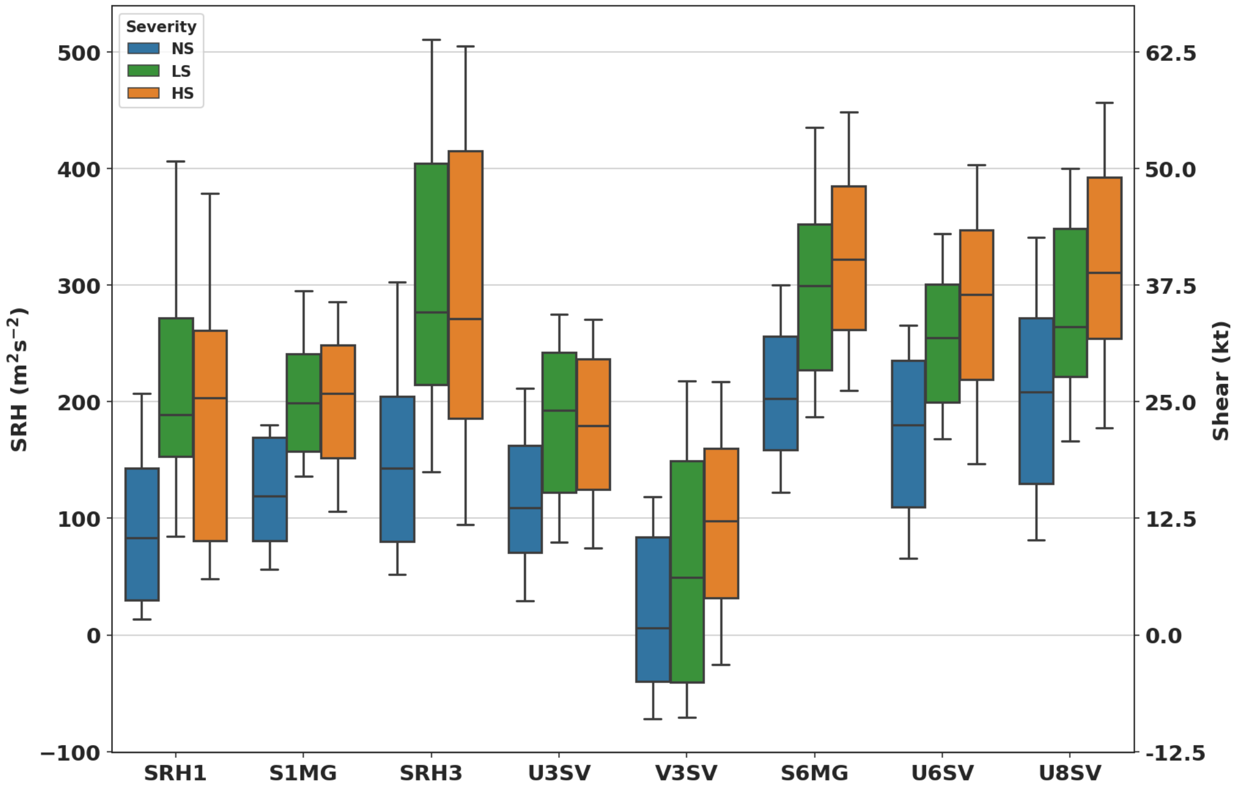

Figure 2: Box-and-whiskers plots for all cases of SRH1 and SHR3 (values plotted along the left axis), and S1MG, U3SV, V3SV, U6SV, S6MG, and U8SV (values plotted along the right axis). Each color-filled box represents the results for NS (blue), LS (green), and HS (orange). The whiskers span the interval from the 10th to 90th percentiles and the boxes enclose the 25th to 75th percentiles. Outliers, or points outside the whiskers, are not plotted.

Accepted for publication in *Weather and Forecasting*. DOI 10.1175/WAF-D-20-0137.1.

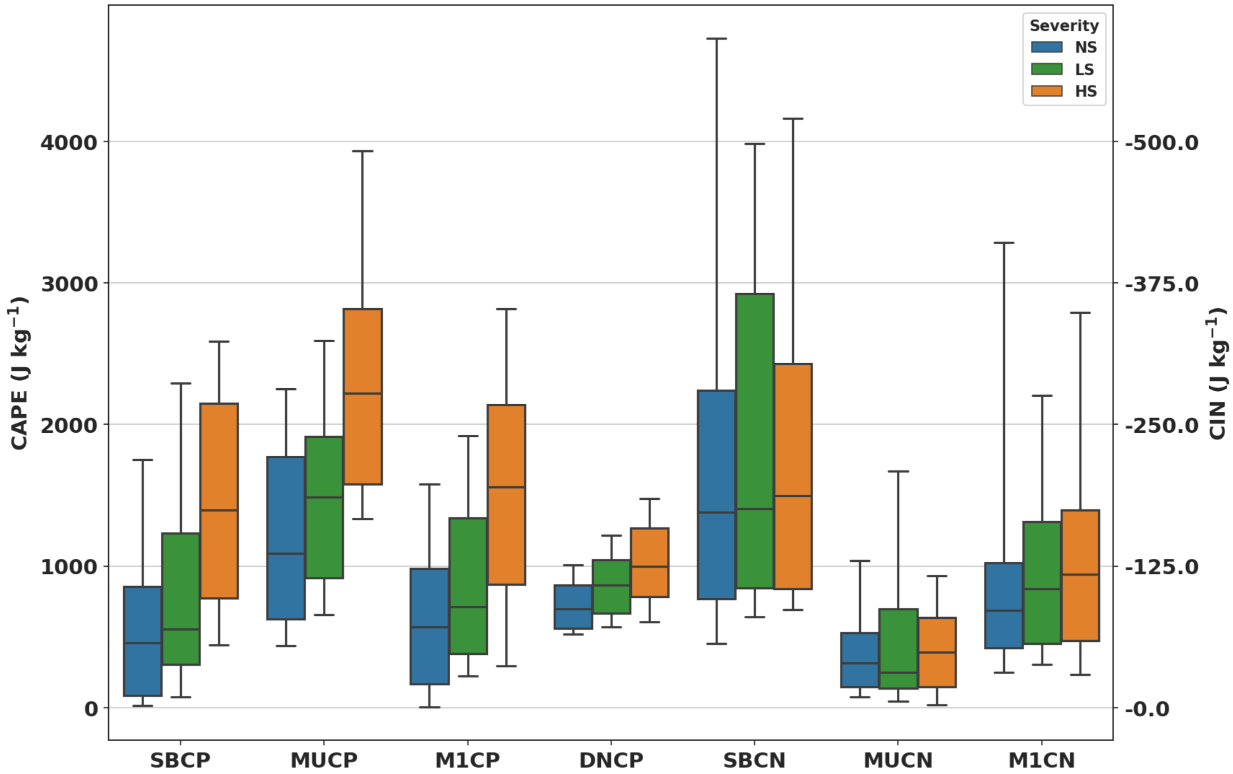

Figure 3: As in Fig. 1, but for SBCP, MUCP, M1CP, DNCP (values plotted along the left axis), and SBCN, MUCN, and M1CN (values plotted along the right axis).

Accepted for publication in *Weather and Forecasting*. DOI 10.1175/WAF-D-20-0137.1.

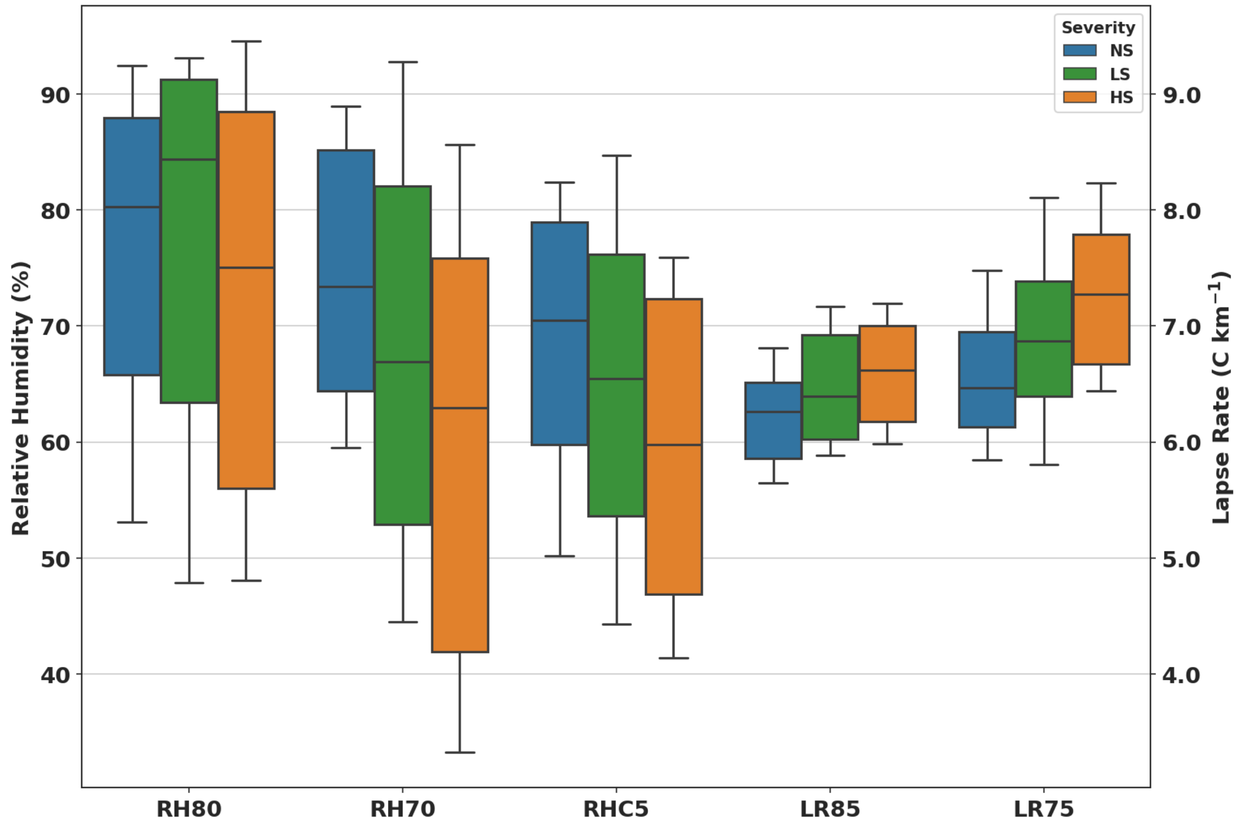

Figure 4: As in Fig. 1, but for RH80, RH70, and RHC5 (values plotted along the left axis), and LR85 and LR75 (values plotted along the right axis).

Accepted for publication in *Weather and Forecasting*. DOI 10.1175/WAF-D-20-0137.1.

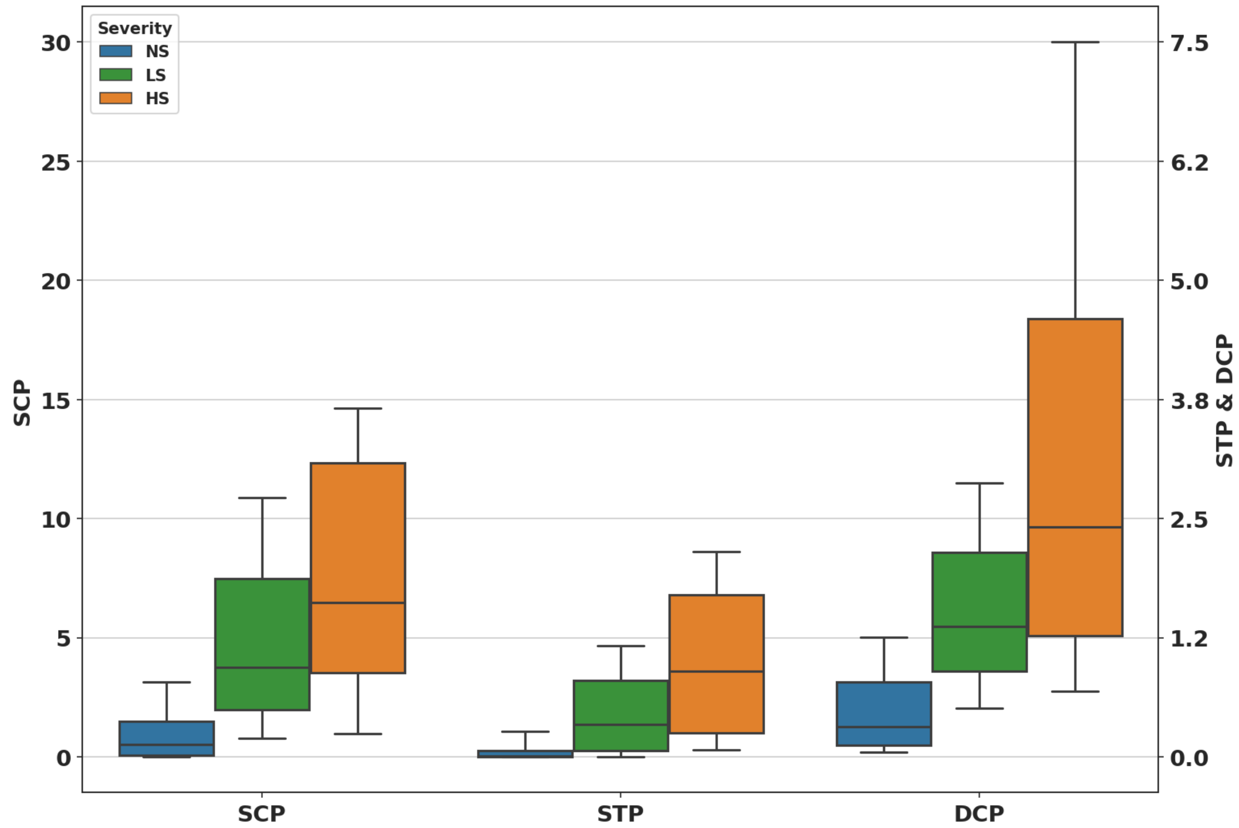

Figure 5: As in Fig. 1, but for SCP (values plotted along the left axis), and STP and DCP (values plotted along the right axis).

Accepted for publication in *Weather and Forecasting*. DOI 10.1175/WAF-D-20-0137.1.

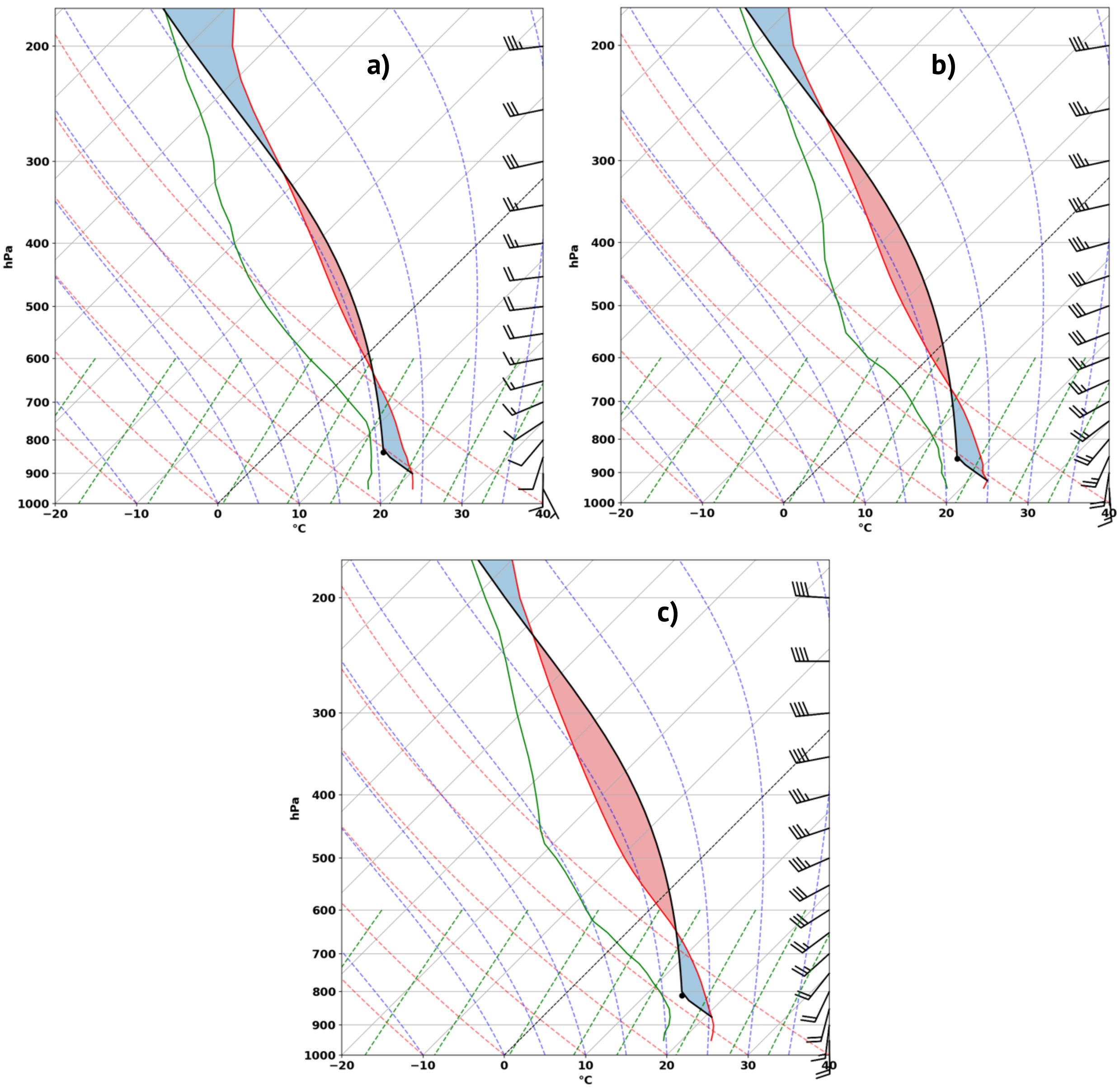

Figure 6: Skew T-Log*p* sounding diagrams for (a) NS, (b) LS, and (c) HS environments, created by averaging all cases for each type. Temperature (red), dewpoint (green), and most unstable parcel (black) profiles are plotted, along with winds on the right side, dry adiabats (dashed red), moist adiabats (dashed blue), and constant mixing ratio lines (dashed green). MUCAPE and MUCIN are indicated by the shaded red and blue areas, respectively.

Accepted for publication in *Weather and Forecasting*. DOI 10.1175/WAF-D-20-0137.1.

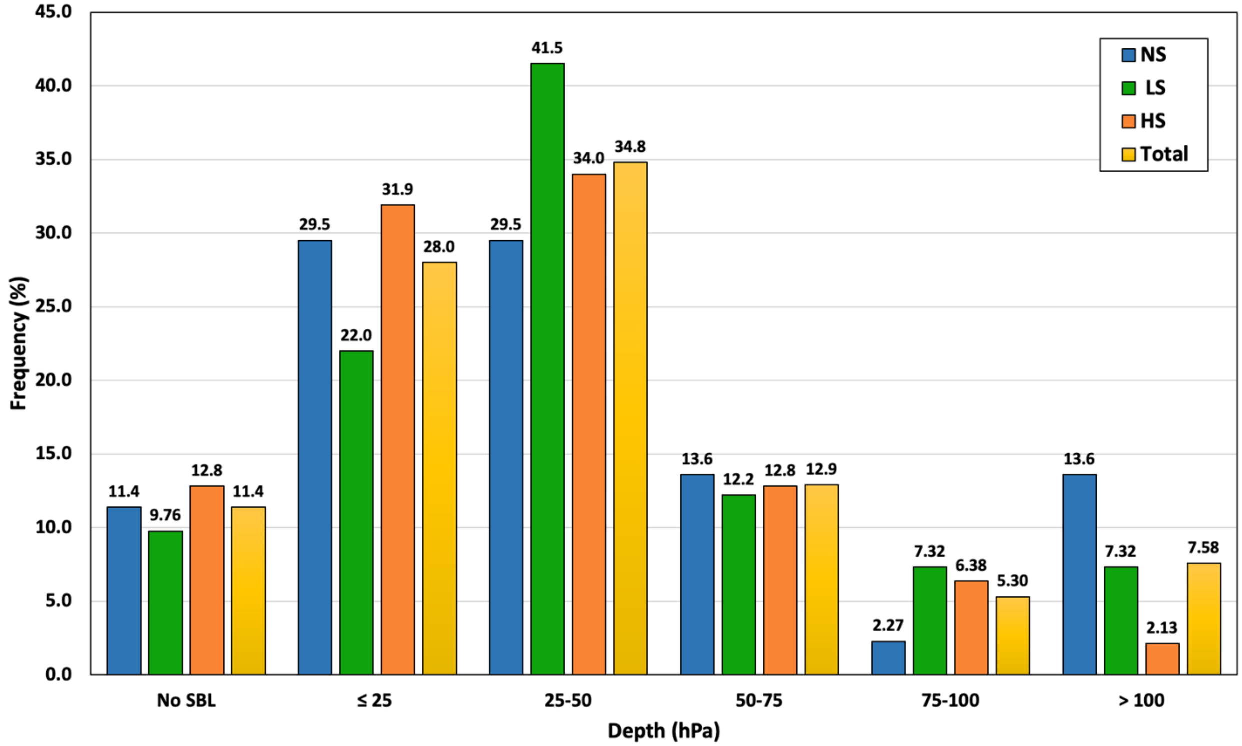

Figure 7: Frequency of occurrence (in %) of SBLs of specified depth (in hPa) for all severity categories. For each interval the largest depth is inclusive, while the lowest is exclusive. Percentages are calculated with respect to the total number of NS (blue), LS (green), and HS (orange) events, and the total sum of all cases (yellow), respectively.

Accepted for publication in *Weather and Forecasting*. DOI 10.1175/WAF-D-20-0137.1.

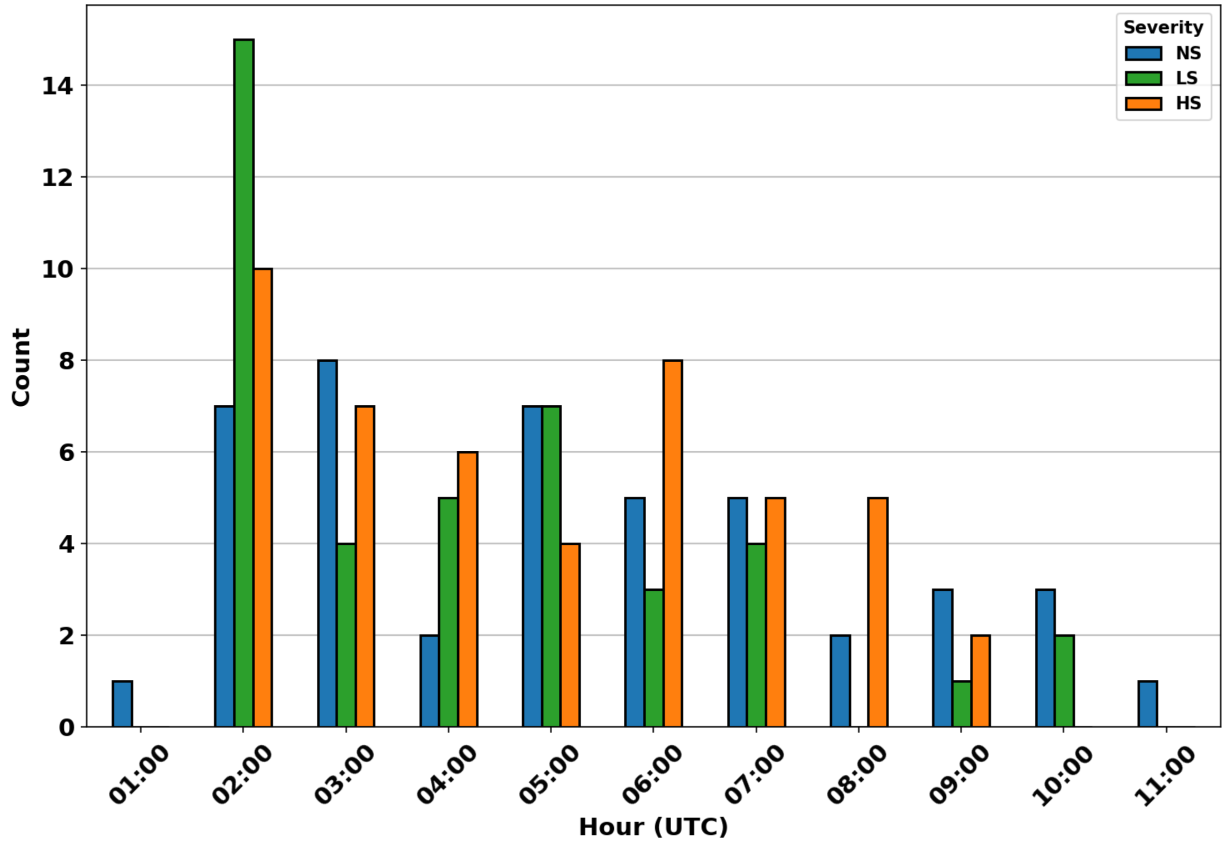

Figure 8: Nocturnal distribution of NS (blue), LS (green), and HS (orange) events by hour of mesoanalysis data used.

Accepted for publication in *Weather and Forecasting*. DOI 10.1175/WAF-D-20-0137.1.

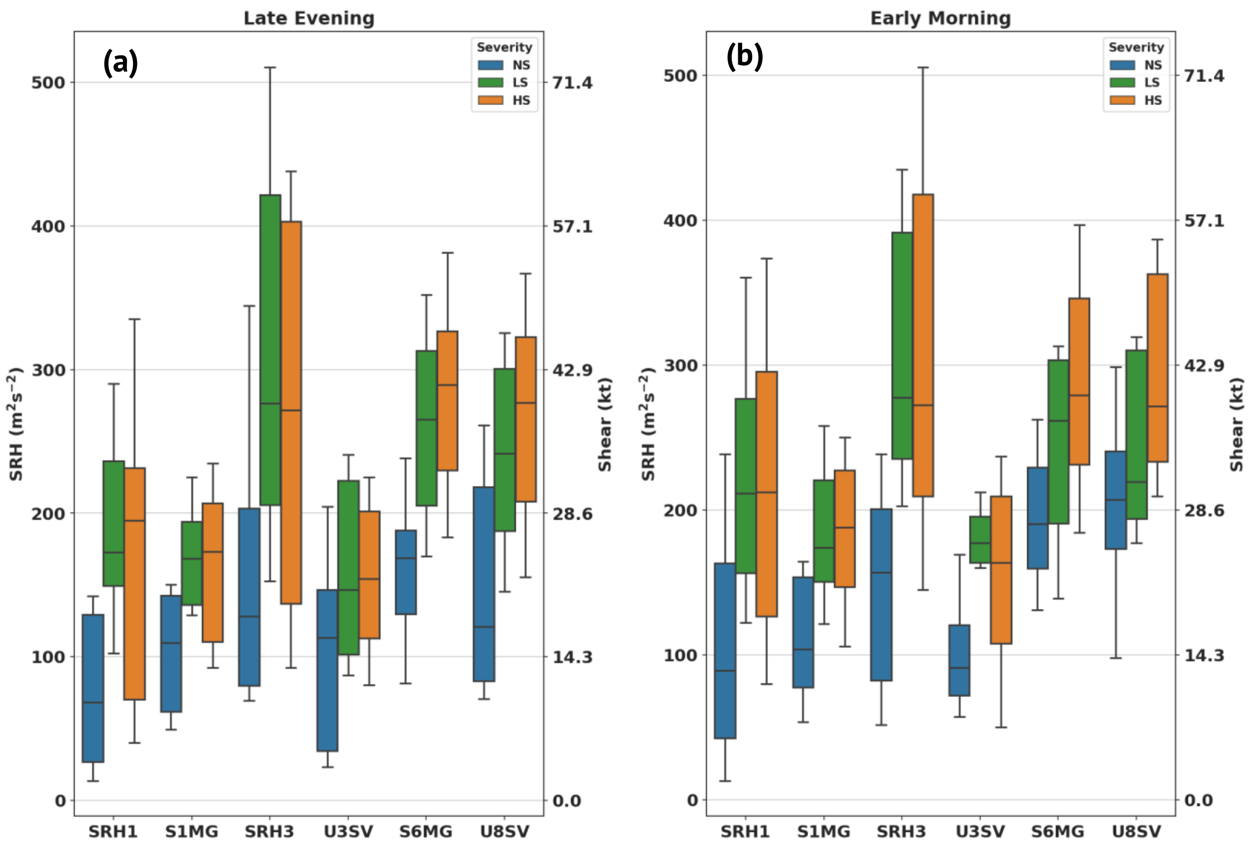

Figure 9: As in Fig. 2, but for SRH1 and SHR3 (values plotted along the left axis), and S1MG, U3SV, S6MG, and U8SV (values plotted along the right axis) for (a) late evening and (b) early morning.

Accepted for publication in *Weather and Forecasting*. DOI 10.1175/WAF-D-20-0137.1.

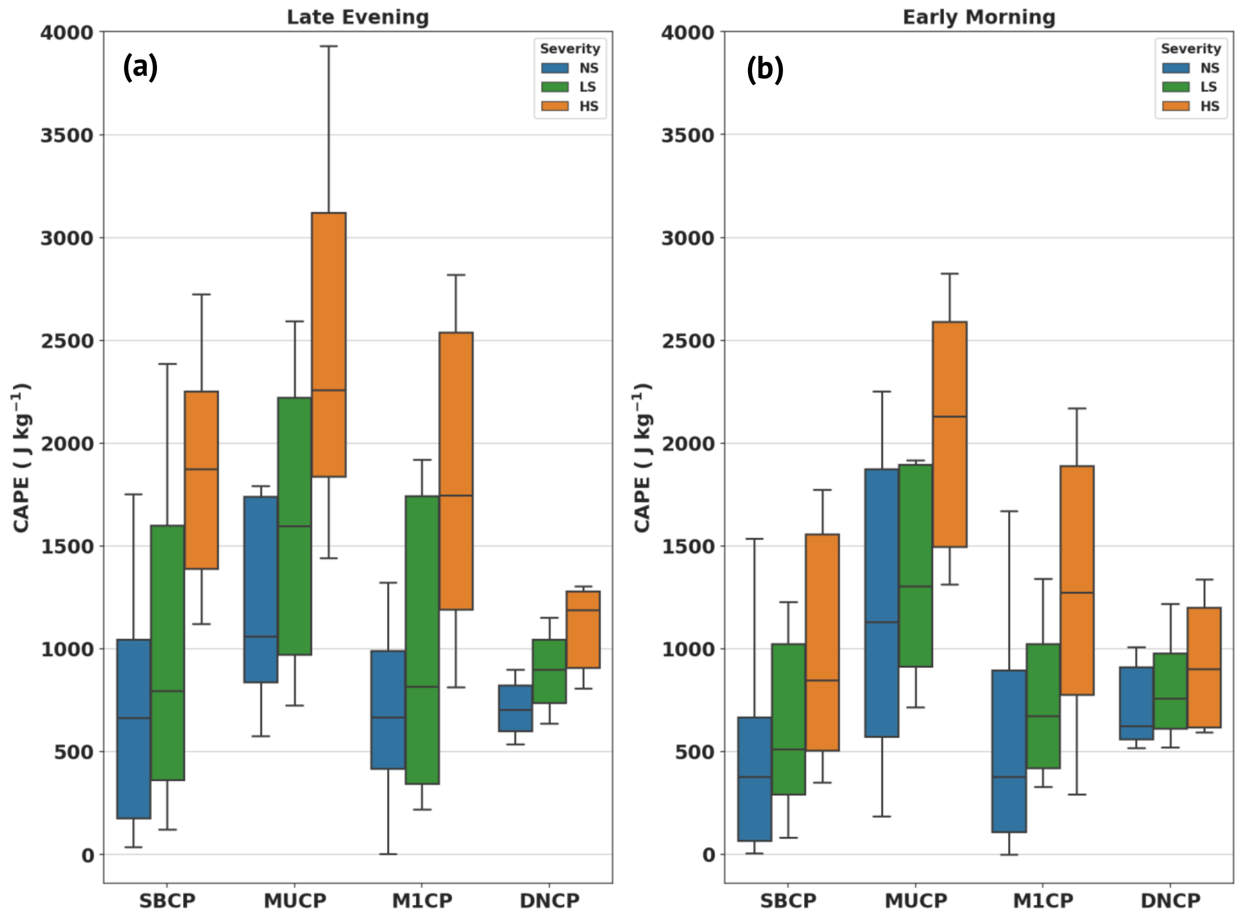

Figure 10: As in Fig. 3, but only for SBCP, MUCP, M1CP, and DNCP for (a) late evening and (b) early morning.

Accepted for publication in *Weather and Forecasting*. DOI 10.1175/WAF-D-20-0137.1.

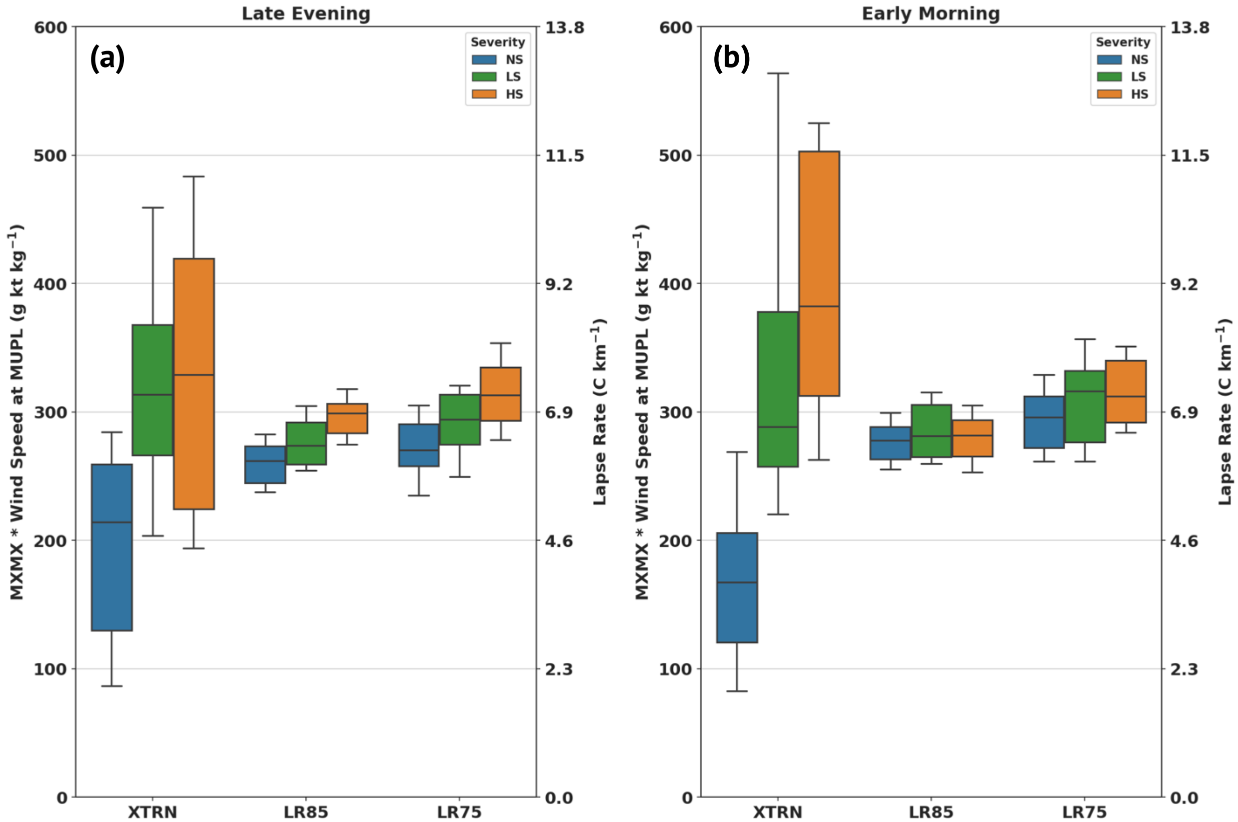

Figure 11: As in Fig. 4, but only for XTRN (values plotted along the left axis), and LR85 and LR75 (values plotted along the right axis), for (a) late evening and (b) early morning.

Accepted for publication in *Weather and Forecasting*. DOI 10.1175/WAF-D-20-0137.1.

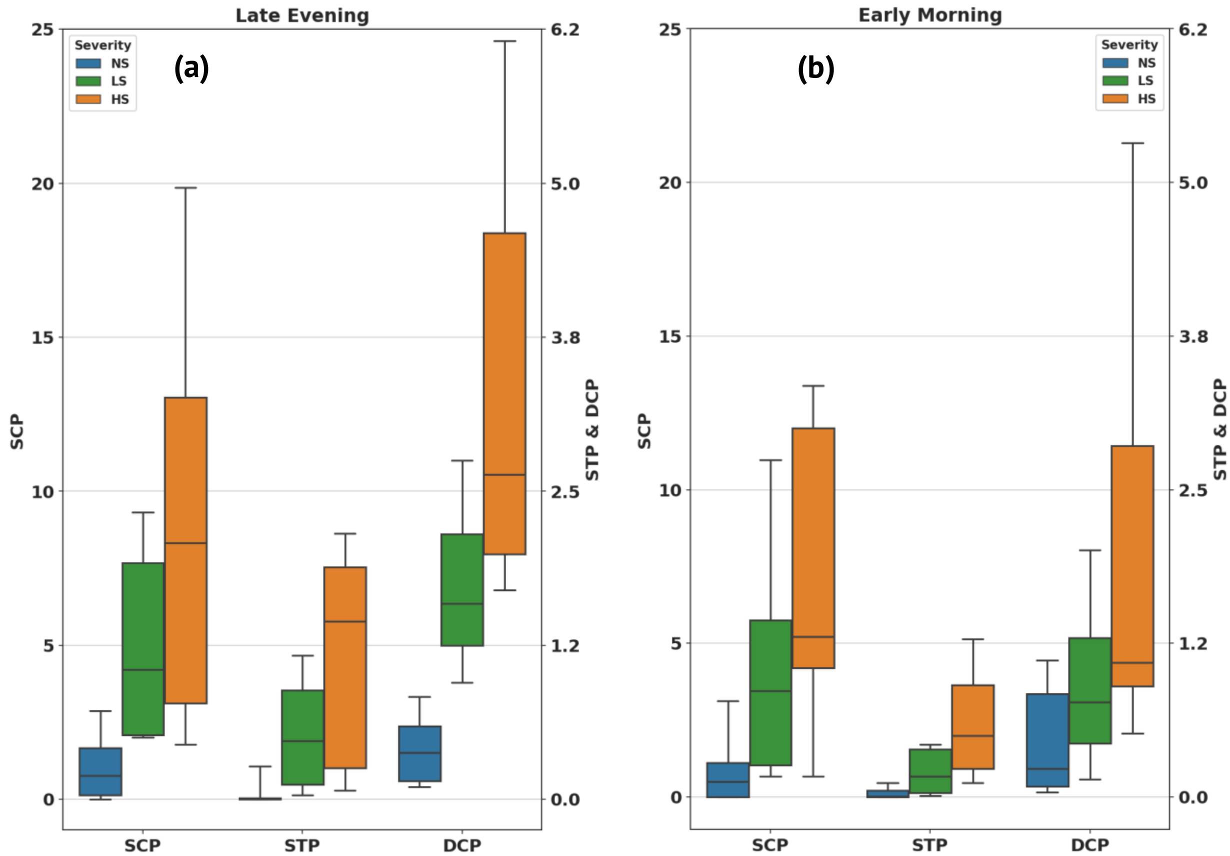

Figure 12: As in Fig. 5, but for (a) late evening and (b) early morning.

Accepted for publication in *Weather and Forecasting.* DOI 10.1175/WAF-D-20-0137.1.

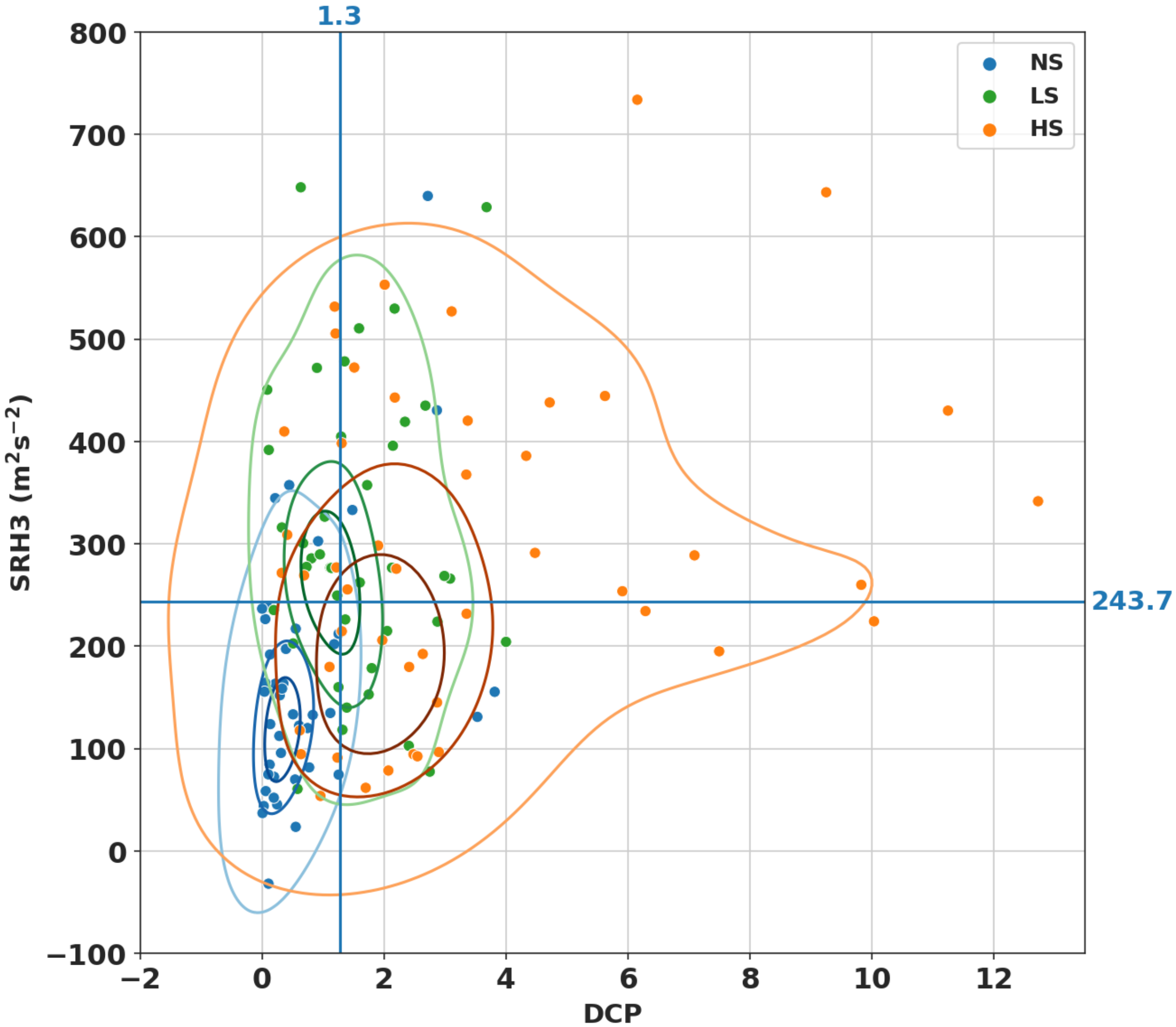

Figure 13: Scatter plot of DCP vs SRH3 with GDKE (Gaussian kernel density estimation) contours overlaid for all severity types (NS in blue, LS in green, and HS in orange). The three GKDE contours for each severity type encompass the top 10% (innermost contour), top 25%, and top 75% (outermost contour) densest points. The vertical and horizontal blue lines indicate the two optimal thresholds associated with the highest HSS values for prediction of NS events for DCP and SRH3, respectively.

Accepted for publication in *Weather and Forecasting.* DOI 10.1175/WAF-D-20-0137.1.

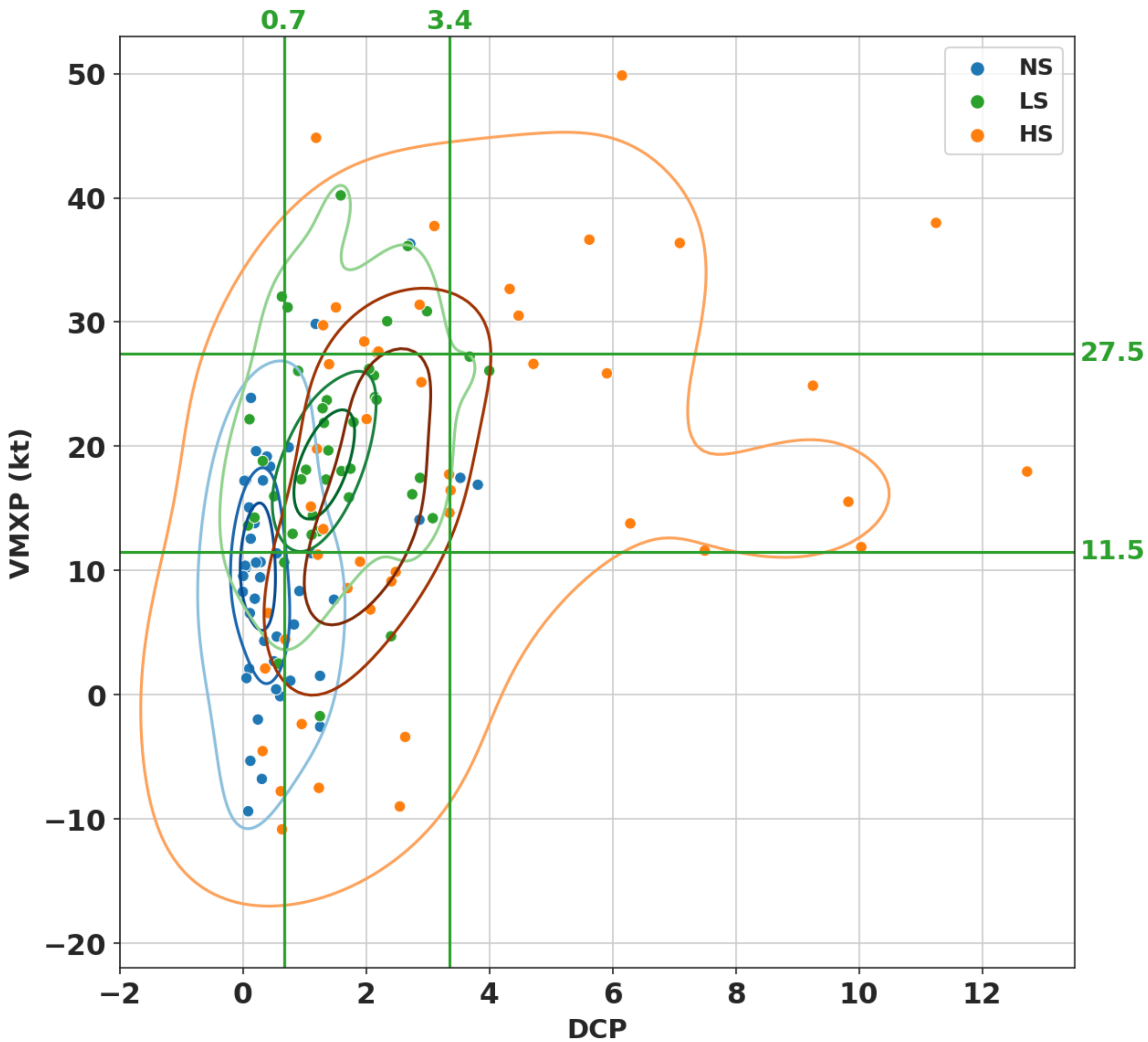

Figure 14: As in Fig. 13, but for DCP vs VMXP. The vertical and horizontal green lines indicate the two optimal lower and upper thresholds associated with the highest HSS values for prediction of LS events for DCP and VMXP, respectively.

Accepted for publication in *Weather and Forecasting*. DOI 10.1175/WAF-D-20-0137.1.

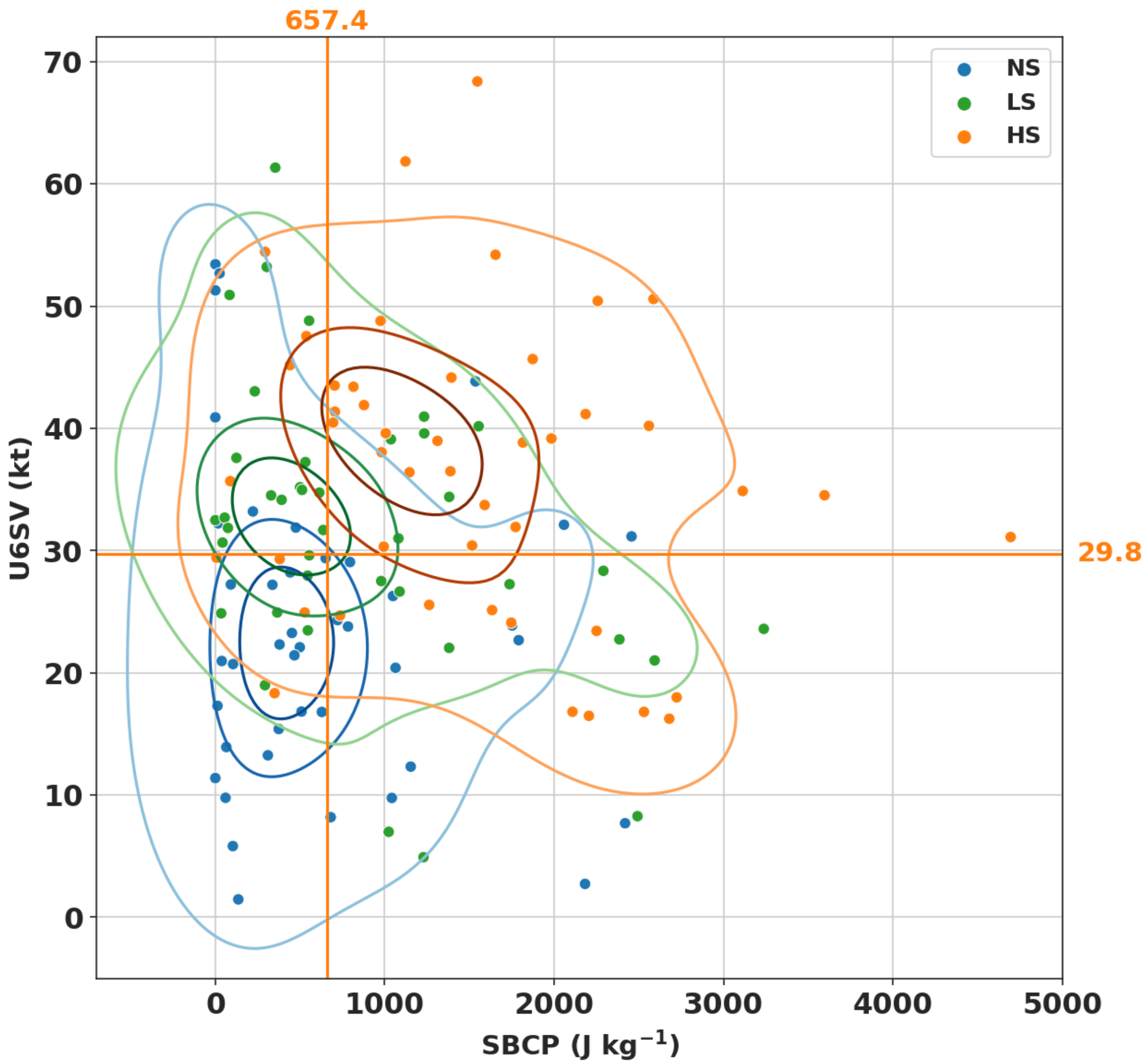

Figure 15: As in Fig. 13, but for SBCP vs U6SV. The vertical and horizontal orange lines indicate the two optimal thresholds associated with the highest HSS values for prediction of HS events for SBCP and U6SV, respectively.

Accepted for publication in *Weather and Forecasting*. DOI 10.1175/WAF-D-20-0137.1.